**Title**

Further exploration of the structure-activity relationship of dual soluble epoxide hydrolase/fatty acid amide hydrolase inhibitors

**Permalink**

https://escholarship.org/uc/item/0tm4d085

**Authors**

Wilt, Stephanie
Kodani, Sean
Valencia, Leah
et al.

**Publication Date**

2021-12-01

**DOI**

10.1016/j.bmc.2021.116507

Peer reviewed

# Further Exploration of the Structure-Activity Relationship of Dual Soluble Epoxide Hydrolase/Fatty Acid Amide Hydrolase Inhibitors

Stephanie Wilt[1], Sean Kodani[2], Leah Valencia[1], Paula K. Hudson[1], Stephanie Sanchez[3], Taylor Quintana[3], Christophe Morisseau[2], Bruce D. Hammock[2], Ram Kandasamy[3,*], Stevan Pecic[1,*]

[1]Department of Chemistry & Biochemistry, California State University, Fullerton, 800 N. State College, Fullerton, CA 92834, United States.

[2]Department of Entomology and Nematology, and UCD Comprehensive Cancer Center, University of California Davis, Davis, CA 95616, United States.

[3]Department of Psychology, California State University, East Bay, 25800 Carlos Bee Blvd. Science S229, Hayward, CA 94542, United States.

## Abstract

Fatty acid amide hydrolase (FAAH) is a membrane protein that hydrolyzes endocannabinoids, and its inhibition produces analgesic and anti-inflammatory effects. The soluble epoxide hydrolase (sEH) hydrolyzes epoxyeicosatrienoic acids (EETs) to dihydroxyeicosatetraenoic acids. EETs have anti-inflammatory and inflammation resolving properties, thus inhibition of sEH consequently reduces inflammation. Concurrent inhibition of both enzymes may represent a novel approach in the treatment of chronic pain. Drugs with multiple targets can provide a superior therapeutic effect and a decrease in side effects compared to ligands with single targets. Previously, microwave-assisted methodologies were employed to synthesize libraries of benzothiazole analogs from which high affinity dual inhibitors (e.g. **3**, sEH $IC_{50}$ = 9.6 nM; FAAH $IC_{50}$ = 7 nM) were identified. Here, our structure-activity relationship studies revealed that the 4-phenylthiazole moiety is well tolerated by both enzymes, producing excellent inhibition potencies in the low nanomolar range (e.g. **6o**, sEH $IC_{50}$ = 2.5 nM; FAAH $IC_{50}$ = 9.8 nM). Docking experiments show that the new class of dual inhibitors bind within the catalytic sites of both enzymes. Prediction of several pharmacokinetic/pharmacodynamic properties suggest that these new dual inhibitors are good candidates for further *in vivo* evaluation. Finally, dual inhibitor **3** was tested in the Formalin Test, a rat model of acute inflammatory pain. The data indicate that **3** produces antinociception against the inflammatory phase of the Formalin Test *in vivo* and is metabolically stable following intraperitoneal administration in male rats. Further, antinociception produced by **3** is comparable to that of ketoprofen, a traditional nonsteroidal anti-inflammatory drug. The results presented here will help toward the long-term goal of developing novel non-opioid therapeutics for pain management.

---

*Authors to whom correspondence should be addressed.

## Introduction

Chronic pain, which impacts between 7% and 55% of people, is described as pain that occurs for longer than six months.[1, 2] Despite decades of research on the mechanisms and determinants underlying pain, opioid analgesics (e.g., morphine, fentanyl) remain the best treatments. However, their use is accompanied by a wide range of dangerous and unpleasant side effects including constipation, sedation, and addiction. The rewarding effects of opioids has fueled the opioid crisis, which has garnered significant interest in the search of novel non-opioid pharmacological treatments for pain.

Inflammation is a part of the immune response triggered by both intrinsic and extrinsic injury.[3] Chronic inflammation, which may be a result of unresolved acute inflammation or sustained chronic injury, can contribute to the progression of multiple chronic diseases including pain.[4] Pain and inflammation often correlate because inflammatory cells are present in those experiencing pain and are thought to act as pain modulators.[5, 6] Anti-inflammatory drugs currently on the market, including aspirin and acetaminophen, are commonly prescribed for those with chronic pain. However, many of them carry undesirable side effects including gastrointestinal ulcers and liver toxicity.[7, 8]

Soluble epoxide hydrolase (sEH) regulates a set of anti-inflammatory signaling lipids called epoxyeicostrienoic acids (EETs).[9, 10] EETs are produced from epoxidation of a double bond in arachidonic acid (AA) by cytochrome P450 (CYP) enzymes (Fig. 1). The sEH hydrolyzes these epoxides to the less bioactive and sometime proinflammatory dihydroxyeicosatrienoic acids.[11, 12] sEH is found widely throughout the human body and its elevation has been associated with inflammatory diseases including metabolic syndrome and neuroinflammatory disorders.[13, 14] Pharmacologic treatment of mouse models of inflammation with sEH inhibitors has been shown to decrease proinflammatory cytokines and increase pro-resolving lipoxins.[15] Additionally, sEH inhibitors reduce inflammatory and non-inflammatory forms of pain in multiple animal models.[16–18]

By comparison, fatty acid amide hydrolase (FAAH) has a similar role in regulating inflammation and pain. It is an integral membrane enzyme that hydrolyzes the endocannabinoid anandamide (AEA) to arachidonic acid (Fig. 1).[19] Anandamide binds to the cannabinoid receptors, $CB_1R$ and $CB_2R$, to elicit its analgesic and anti-inflammatory effects.[20–23] Inhibiting FAAH is effective at reducing inflammatory and non-inflammatory pain in a number of models, but it was not effective at reducing pain in human clinical trials.[24] In addition, there is some evidence that AEA and other *N*-acyl ethanolamides might be substrates for CYP enzymes.[23, 25, 26]

Interestingly, both sEH and FAAH enzymes convert bioactive endogenous anti-inflammatory and analgesic agents, EETs and anandamide, respectively, by hydrolysis to inactive metabolites.

In a study by *Sasso et al.* (2015), concurrent inhibition of FAAH and sEH synergistically reduced pain in both inflammatory and neuropathic rodent pain.[27] Given this synergy, dual sEH/FAAH inhibition is an attractive approach for treating pain with minimal side effects. This approach of inhibiting multiple targets is also known as polypharmacology and can be beneficial to both increase efficacy and decrease off-target effects.[28] Designed Multiple Ligands (DMLs) are small molecules designed to simultaneously interact with several biological targets involved in the disease.[29] In addition to the benefits of pharmacology, they have the added advantage of simplified dosing and pharmacokinetics. This approach has been successfully utilized in several medicinal chemistry programs. For example, Palermo et al. have successfully designed and synthesized a dual inhibitor of the FAAH and cyclooxygenase (COX) enzymes, by combining the pharmacophoric elements needed to block FAAH and COX in a single scaffold.[30] In a recent study, the dual inhibitor of sEH and COX-2 was discovered by linking pharmacophoric moiety of celecoxib (a known COX-2 inhibitor) with the adamantyl-urea moiety present in a potent sEH inhibitor AUDA.[31] Based on the demonstrated synergy between FAAH and sEH inhibitors, we decided to design dual inhibitors for these two enzymes (Fig. 1). In our previous work[32], we were able to identify a common pharmacophore for both targets. This pharmacophore featured a phenyl ring connected via amide bond to a piperidine moiety, which is connected via sulfonamide bond to the modified aromatic ring located on the right side of the molecule (Fig. 2). This SAR led to the discovery of several potent dual FAAH/sEH benzothiazole-based inhibitors.

Herein, we expand on those studies by investigating the role of the benzothiazole moiety on the dual FAAH/sEH inhibition potencies and examine the effects of dual sEH/FAAH inhibition in a rat model of acute inflammatory pain.

## Results and Discussion

### - Design and Synthesis

Our design of new dual inhibitors was guided by several rationales. Previously, *Wang et al.* (2009) explored the methylbenzothiazole ring on the left side of the pharmacophore (phenyl ring-amide-piperidine moiety-sulfonamide bond, shown in red in Fig. 2). The most potent FAAH inhibitor in this study, **1**, demonstrated the importance of this bulky hydrophobic system for the potent inhibition at the active site of the rat FAAH enzyme. In separate studies, it was observed that the bulky, hydrophobic groups on the left-hand side of sEH inhibitors, represented with **2**, are important for modulating human sEH enzymes[33, 34]. We decided to keep the benzothiazole ring on the left side of the pharmacophore and investigated the SAR of the aromatic ring bound to the sulfonamide group.[32] In short, our SAR showed that halogens (fluoro-, chloro- and bromo-) and methyl-groups, placed at the *ortho* and at both *ortho/para* positions, are all well tolerated in the human FAAH and human sEH enzymes leading to low nanomolar inhibition potencies on both enzymes. The molecular docking experiments revealed that these dual inhibitors interact within catalytic sites of both enzymes. The most potent compound identified in this study, **3**

(Fig. 2), had high potency for human FAAH ($IC_{50}$ = 7 nM) and human sEH ($IC_{50}$ = 9.6 nM). This potency is probably due to Van der Waals interactions in the substrate binding pockets and hydrogen bonding with either enzyme's catalytic triad, S241-S217-K142 and Y383-Y466-D335 in FAAH and sEH catalytic sites, respectively (see Molecular Modeling section). Although we were able to identify several highly potent dual inhibitors, these all possess very similar structural features and similar predicted pharmacokinetic and pharmacodynamic properties. Unfavorable absorption, distribution, metabolism, excretion, and toxicology (ADMET) properties have been identified as a major cause of drug candidate failure in the pharmaceutical industry.[35] ADMET properties are expensive to perform and difficult to model due to biological complexity, and no single approach can be used to predict the full range of ADMET properties that are desired.[36] Thus, we decided to further explore the chemical space important for dual inhibition and discover new scaffolds that will in turn provide diverse ADMET properties. In addition, this new SAR knowledge will positively impact basic science knowledge in the drug discovery and drug design fields. In a separate study, we were able to utilize the 4-phenylthiazole moiety whose framework was previously examined by *Wang et al.* (2009) and were able to incorporate it in several potent FAAH inhibitors.[37, 38] Using information obtained from these above mentioned SAR studies in combination with molecular modeling and crystallography data, we decided to explore whether modifying the benzothiazole moiety can affect inhibitory potency. To evaluate the effect of this group on the inhibitory capacity of the dual inhibitors, we kept the 2-chlorophenyl group connected to the sulfonamide bond of the pharmacophore and synthesized 16 analogs with various groups on the left side of the molecule (Fig. 2). To explore the importance of the benzothiazole functionality on the activity, we prepared 3 different classes of analogs (Table 1). The first group consists of 7 compounds, **6a-g**, that utilize a simplification strategy where the benzothiazole part was replaced with smaller groups. Next, the second group of analogs, **6h-k**, was designed using bio-isostere and/or ring variations and varying alkyl substituents strategies. Finally, the third group represented with five analogs, **6l-p**, was designed to determine the importance of the 4-phenylthiazole moiety in the activity for both enzymes. As shown in Scheme 1, using previously established procedures[39], starting from commercially available methyl isonipecotate and 2-chlorobenzenesulfonyl chloride, sulfonamide **4** was obtained in 74% yield via a coupling reaction with Hünig's base and microwave irradiation. Saponification of the methyl ester with a 2 M aqueous solution of lithium hydroxide furnished the carboxylic acid **5** in 91% yield. Compound **5** was subsequently coupled with different anilines under standard EDC peptide coupling conditions and microwave irradiation yielding compounds **6a** to **6k** in moderate yields. Five different 4-phenylthiazole anilines, **7l-p** (inner box in Scheme 1), were also prepared by condensation of the commercially available 4-aminothiobenzamide and various 2-bromoacetophenones and subsequently coupling them with **5** yielding final compounds **6l** to **6p** in moderate yields.

## - Biological evaluation

The potency of the newly designed and synthesized analogs **6a-p** was assessed against both human FAAH and human sEH (Table 1). The SAR study started with a first set of analogs, **6a-g**, designed using simplification tactics to test whether the benzothiazole ring is an essential part of the pharmacophore. The first analog, **6a**, possessing no substituent on

the phenyl ring of the pharmacophore, showed complete loss of inhibition potency at the human sEH enzyme, but led to moderate inhibition potency on the human FAAH enzyme with an $IC_{50}$ of 510 nM. Placement of fluoro-, chloro-, bromo- and methyl groups (**6b**, **6c**, **6d**, and **6e**, respectively) at the *para* position of the phenyl group in the pharmacophore did not restore any potency against sEH, but improved the inhibition potencies against human FAAH with $IC_{50}$s in the 100–200s nM range. The introduction of the bulkier and more polar thiazole ring, **6f**, led to a significant improvement in the inhibition potency of the human sEH enzyme ($IC_{50}$= 9.2 nM), and comparable inhibitory potency on the human FAAH enzyme to the **6b-e** analogs. Interestingly, the introduction of the oxazole rings, **6g**, did not have much of an effect on the inhibitory potency on human FAAH ($IC_{50}$ = 140 nM) while reducing sEH inhibitory potency 20-fold ($IC_{50}$ = 180 nM) relative to the thiazole analog **6f**. This result could be explained with the difference in the steric/electronic properties of the sulfur atom compared to the oxygen and implies that sulfur (more bulky and less electronegative) has greater surface area resulting in closer Van der Waals interactions. The next set of analogs, **6h-k**, were aimed to test whether the benzothiazole bioisosteres may have improved potency relative to the reference compound, **3**. First, a methyl group was introduced at position 6 of the benzothiazole ring. The methyl group did not affect the binding of the benzothiazole moiety and **6h** showed excellent inhibition potencies with both enzymes, human FAAH ($IC_{50}$= 1.8 nM) and human sEH ($IC_{50}$= 8.7 nM). The replacement of the benzothiazole ring with *N*-methylbenzoimidazole, **6i**, led to diminished inhibitory potency on both enzymes. On the other hand, placement of the benzooxathiol moiety, **6j**, was well tolerated in the human sEH ($IC_{50}$= 22.7 nM) and has shown moderate inhibition potency on the human FAAH ($IC_{50}$ = 142 nM). With the design of analog **6k**, we decided to extend the alkyl linker to the aromatic moiety and this strategy led to complete loss of inhibition potency on the human FAAH, while this change was well-tolerated by the human sEH enzyme ($IC_{50}$ = 170 nM). The third set of analogs, **6l-p**, explored the potency of the 4-phenylthiazole moiety on both enzymes. All five analogs showed excellent inhibition potencies in the low nanomolar range with both enzymes. This suggests that analogs with this bulky moiety on the left side of the pharmacophore are favored in the active sites of both enzymes and are important for the potent dual inhibition. Most compounds pursued as FAAH inhibitors have been irreversible covalent inhibitors.[40] Indeed, in the last several years, the majority of the research has been focused on developing irreversible covalent FAAH inhibitors, largely because an irreversibly inhibited FAAH would not be affected by accumulations of its substrate, anandamide.[41] In fact, the known FAAH inhibitor, URB 597, the same one we used as a reference compound in this study, operates via carbamoylation of the catalytic serine residue (S241) in the active site of FAAH.[42] Inhibition through carbamoylation mechanism is time-dependent because the inhibitory potency depends on the rate of this mechanism and thus increases the $IC_{50}$ with longer incubation times.[43] Using this principle, we decided to elucidate the type of inhibition for the previously discovered dual inhibitor **3** and one of 4-phenylthiazole analogs, **6o**. We noticed that the potencies of both **3** and **6o** do not change with time (Supplemental, Table S1), while the control URB 597 showed significant increase in potency over the same period. These findings suggest that **3** and **6o** (and most likely other 4-phenylthiazole analogs identified in this study) are probably inhibiting FAAH in a reversible manner (i.e., are not to forming a covalent bond with S241). However, to fully investigate the mode of noncovalent inhibition (competitive or mixed) of

this set of inhibitors, we will need to perform more kinetic analyses which will be addressed in our future follow-up studies.

## - Molecular Modeling Studies

Molecular docking experiments were performed to better understand the binding modes of dual inhibitors. We previously reported the preparation and validation of the homology model of the human FAAH enzyme[37] since the X-Ray crystallographic structure is not available. The crystal structure of human sEH complexed with the piperidine-amide inhibitor is available at RCSB Protein Data Bank (PDB: 4HAI). Using ICM Pro software, all compounds were docked in both the human FAAH homology model and human sEH model. The ICM Pro docking scores (Table 1) represent unitless approximations of the binding free energy between the ligand (inhibitor) and the enzyme where lower docking scores (especially below −30) suggest a higher chance that the inhibitor is bound to the enzyme. Our main goal is to determine whether docking scores obtained in these docking experiments could be correlated with in vitro results. Further, if scoring is reliable, we could use Virtual Ligand Screening in the future design of dual inhibitors. There was not complete correlation between the *in vitro* results and docking scores (Supplemental, Figs. S1 and S2); however, all potent dual inhibitors with the 4-phenylthiazole moiety, **6l-p**, have docking scores below −30. The poor correlation between predicted affinities and experimentally determined affinities is quite common in molecular modeling experiments.[47] There are many factors that affect the reliability of pose predictions and scoring, and some molecular modeling software appear to better perform on hydrophobic vs. hydrophilic pockets, some are better with small molecules vs. peptides, etc.[48] Since we noticed an agreement in scoring with in vitro results for 4-phenylthiazole analogs, we will still be able to use docking scores in the future design of at least this set of dual inhibitors. This will be tested in our follow-up experiments. For obtaining the docking poses of ligands in the enzyme binding pockets, ICM Molsoft software is using several different interaction potentials, such as van der Waals potentials, optimized electrostatic term, hydrophobic term and loan-pair-based potential (which is involved in hydrogen bonding). Conformational sampling is based on the biased probability Monte Carlo (BPMC) procedure.[49] This approach has been validated in many medicinal chemistry settings.[50–52] We started our docking experiments by first docking the known FAAH and sEH inhibitors, URB-597 and AUDA, respectively (Supplemental, Figs. S1-S4). All important interactions of these inhibitors with the residues within active sites are present in our model and are in agreement with the previously reported models.[9, 53] Next, we focused our attention on to visual inspection of the binding poses of the 4-phenylthiazole set of analogs within both sEH and FAAH active sites. We selected dual inhibitor **6o** as a representative compound from this series to analyze binding modes in more details and to try to define the pharmacophore needed for dual binding. As shown in Figs. 3A and 3B, the inhibitory potency of **6o** within the human FAAH binding site is based on several intermolecular interactions: a possible hydrogen bonding between G485 and -NH- (as a hydrogen bond donor) and many non-polar and hydrophobic interactions (Supplemental, Table S2). The 2-chlorophenyl ring of the inhibitor **6o** is found to be embedded between several hydrophobic and aromatic amino acid residues (Y194, I238, L380, F381, L433, V491 and F432). The piperidine part interacts with F192 and L404, while the aromatic 4-phenylthiazole moiety forms several important non-covalent interactions with Y194, L429,

V422, I530 and W531, which we believe all contribute to high inhibitory potency of this analog. We noticed that the 4-phenylthiazole moiety is directed towards the large deep pocket (broken thick line around 4-methylphenyl ring in Fig. 3A represents the accessible surface) that opens toward the solvent and probably will allow access to many more structural modifications. These will be further explored in our follow-up studies. The dual inhibitor **3** (identified previously) was used to compare its binding pose with the newly identified **6o** from the 4-phenylthiazole series. The visual inspection of the dual inhibitor **3** in the active site of FAAH (Supplemental, Figs. S5 and S6), revealed that this analog shares many same non-polar and hydrophobic interactions similar to **6o**, e.g. S193 in the proximity of the chlorine atom, L404 interacting with the piperidine ring and W531 probably forming π-π interactions with the aromatic rings of benzothiazole moiety (Supplemental, Table S2). Next, we noticed the absence of the hydrogen bond with the G485. However, this dual inhibitor is interacting with both S217 and S241, the two residues that are part of the FAAH catalytic triad (K142-S217-S241)[54], which probably accounts for the high FAAH potency of this inhibitor. The visual inspection of **6o** docked into the human sEH reveals that the potency of this inhibitor is based on Van der Waals interactions and H-bonding interactions within the active site (Figs 4A and 4B). The amide bond of **6o** is in close proximity to two tyrosine residues (Y383 and Y466) and one aspartic acid residue (D335). These three residues are involved in the hydrolysis of the substrate EET in the catalytic pocket of the sEH enzyme.[33] In addition, the dual inhibitor **6o** forms many hydrophobic interactions that probably contribute to the high inhibition potency of this compound (Supplemental, Table S3). The 2-chlorophenyl moiety is surrounded with several aromatic and hydrophobic residues: F387, L408, L417 and W525. The piperidine ring is interacting with Y383, L428 and V498, while the 4-phenyl thiazole is embedded with several hydrophobic residues: W336, Y343, I375, F381, W473 and A476. This suggests that the potency of this inhibitor is primarily based on van der Waals and π-π interactions between the enzyme active site and **6o**. The 4-phenylthiazole moiety is also opened towards the large hydrophobic pocket, suggesting that various additional groups should probably fit there, permitting to expand our SAR knowledge at-large. We also compared the binding modes of the previously identified dual inhibitor **3** within sEH active site (Supplemental, Figs. S7 and S8 and Table S3), with the binding modes of the **6o**. First, we noticed that the nitrogen atom of the amide bond is in the proximity of D335 and is forming hydrogen bond with this residue. Next, we observed the same interactions of the 2-chlorophenyl moiety as in **6o**: F387, L428, L417 and W525, plus the additional L408 interaction. Similarly, piperidine ring possesses same interactions with Y383 and V498, and additional F267 and H524. Finally, the benzothiazole is interacting with W336 and I375, and several additional amino acid residues: M339, P371, M469 and L499. Very similar binding poses, and several shared interactions of both dual inhibitors within binding pockets probably explain the similar high potency of these two inhibitors for both, sEH and FAAH enzymes *in vitro*.

Finally, the chemical space for this set of dual inhibitors is summarized in Fig. 5. To be potent, a dual inhibitor should possess one hydrogen bond donor (shown in blue), four hydrogen bond acceptors (shown in red), the three lipophilic parts- with two located at both ends of the molecule (yellow sphere), and three aromatic parts (shown as grey barrels). The model suggests placement of particular isostere groups within the distances between

the pharmacophore and within these pharmacophoric regions should produce potent dual inhibitors, and our follow-up SAR studies will be guided by the discoveries described here.

### - *In silico* ADMET predictions

Before performing *in vivo* preclinical experiments, several pharmacokinetic and pharmacodynamic properties were predicted *in silico* for the most potent dual inhibitors **6h** and **6l-p**, using the ICM-Pro-Chemist tool (Table 2). We were particularly interested in the Lipinski Rule of Five[55, 56] and Veber's Rule[57]. The Lipinski Rule of Five states that a drug candidate is more likely to exhibit poor absorption if two or more of the following criteria are fulfilled: more than 5 H-bond donors (HBD), more than 10 H-bond acceptors (HBA), the molecular weight is greater than 500 g/mol, and the calculated Log P (CLogP) is greater than 5. However, there are several exceptions to Lipinski's Rule and specifically how it applies to drugs that are being transported into cells by transport proteins located in the cell membrane.[58] On the other hand, Veber's rule does not consider a molecular weight cutoff at 500 as a significant factor for absorption, and suggests that the good oral bioavailability can be predicted by observing the number of rotatable bonds (N of Rot Bonds) and polar surface area (PSA). According to the Veber's rule, a compound having less than 10 rotatable bonds and a PSA equal to or less than 140 Å is considered a good drug candidate in terms of absorption. All six dual inhibitors **6h and 6l-p** have molecular weights slightly above the 500 g/mol cutoff and calculated LogP values are above 5 (Table 2). Nevertheless, these inhibitors have less than 10 HBA, less than 5 HBD, and are not violating either of the two Veber's rule. In addition, the higher molecular weight of the dual inhibitors makes them less likely to cross the blood brain barrier and cause CNS side effects. Next, we ran Caco-2 prediction experiments. The human colon epithelial cancer cell (Caco-2) line model[59] is an established model for prediction of permeability of orally administered drugs and, in turn, the absorption of potential drug candidates. A Caco-2 score higher than −5 suggests a highly permeable drug candidate, while scores below −6 represent a poorly permeable compound. All tested dual inhibitors **6h and 6l-p** have predicted Caco-2 scores between −5 and −6, suggesting they are moderately permeable drug candidates. Therefore, this set of newly discovered dual inhibitors should have good oral bioavailability and the information in Table 2 should be used for formulation in *in vivo* experiments. To access some metabolic parameters, the half-lives of the dual inhibitors **6h and 6l-p** were predicted. The analysis showed that **6l** has the shortest half-life of 1.91 hours while **6p** has the longest predicted half-life of around 3 hours. As a part of the pharmacodynamic analysis, several factors important for the possible toxic effects of the drug candidates were then predicted. Many drugs interact with the cardiac potassium channel encoded by the human ether-a-go-go-related gene (hERG). This interaction can result in lethal cardiac arrhythmias and prediction of this inhibition is a part of the modern drug discovery process.[60, 61] The predicted results show that none of the new dual inhibitors will likely exhibit unwanted hERG inhibition since the predicted hERG score is less than the cutoff value of 0.5 for all tested compounds. To predict the toxic doses of these dual inhibitors, half lethal dose values ($LD_{50}$ values in mg/kg body weight) were predicted (Table 2). According to the globally harmonized system of classification of labelling of chemicals, there are 6 toxicity classes defined with Class I ($LD_{50}$ values   5 mg/kg) as the most toxic and Class VI ($LD_{50}$ values   5000 mg/kg) as relatively non-toxic compounds.[62] Dual inhibitors **6h and 6l-p** belong

to Class IV with values within this class range ($300 < LD_{50}$   2000 mg/kg). Furthermore, the calculated Tox score of 0 predicts that none of the analyzed analogs in this group have potentially toxic functional groups and/or by-products during metabolism. Finally, a "drug-likeness" was calculated for compounds **6h and 6l-p**. This purely empirical value takes together several factors calculated above and describes if the selected compound is a good drug candidate. Scores between −1 and 1 suggest that the tested compound is a good candidate. According to Table 2, all newly described dual inhibitors fall into this range.

### - *in vivo* analysis of antinociception

The most potent dual sEH/FAAH inhibitor identified in our previous study, **3**, was used to demonstrate antinociception following intraperitoneal administration in a rat model of acute inflammatory pain. The Formalin Test[63] is commonly used to evaluate the ability of an analgesic drug to provide relief against acute inflammatory pain. The test involves subcutaneous injection of dilute formalin into the plantar surface of the rat's hindpaw to elicit pain behaviors such as licking and guarding of the injected hindpaw. The time spent licking and guarding is quantified in two distinct phases. The first phase lasts 10 min after injection and involves direct activation of nociceptors.[64] The second phase begins approximately 20 min after injection and is mediated via inflammatory processes, as common nonsteroidal anti-inflammatory drugs block the second, but not the first, phase.[64] Fig. 6A shows pain-related behaviors following injection of **3** and an effective dose of ketoprofen, a traditional nonsteroidal anti-inflammatory drug (NSAID), in the first phase of the Formalin Test. A one-way ANOVA revealed that administration of either a dose of **3** or ketoprofen was ineffective at inhibiting licking and guarding behaviors compared to rats treated with vehicle [$F(3, 20) = 0.187$, $p = 0.90$)]. Fig. 6B shows pain-related behaviors following administration of formalin, **3**, and ketoprofen in the second phase of the Formalin Test. A one-way ANOVA revealed that intraperitoneal administration of **3** and ketoprofen attenuated pain behaviors induced by the intraplantar injection of formalin [$F(3, 20) = 6.834$, $p = 0.002$)]. A Tukey post-hoc test revealed that licking and guarding behaviors were significantly attenuated following administration of the high dose of **3** (1 mg/kg) and ketoprofen (Tukey: Vehicle vs. 1 mg/kg, $p < 0.05$; Vehicle vs. ketoprofen, $p < 0.05$). Administration of the low dose of **3** (0.1 mg/kg) did not attenuate licking and guarding behaviors (Tukey: Vehicle vs. 0.1 mg/kg, $p > 0.05$). Lastly, there was no difference in the magnitude of pain relief produced by 1 mg/kg **3** and 30 mg/kg of ketoprofen (Tukey: 1 mg/kg vs. ketoprofen, $p > 0.05$).

These data provide the first evidence of antinociception following administration of a dual sEH/FAAH inhibitor. Intraperitoneal administration of the higher dose of **3** attenuates licking and guarding behaviors induced by an intraplantar injection of formalin. The lower dose of **3** was ineffective suggesting a dose-dependent relationship in antinociception. The magnitude of antinociception produced by 1 mg/kg of **3** is comparable to antinociception produced by a high dose of ketoprofen (30 mg/kg). The results with ketoprofen are consistent with other studies demonstrating that 30 mg/kg is an effective dose against formalin-induced pain.[65] The differences observed between Phase 1 and Phase 2 of the Formalin Test indicate that **3** produces pain relief in a manner consistent with drugs that prevent pro-inflammatory states such as NSAIDs. NSAIDs such as indomethacin and

naproxen also inhibit pain-related behaviors in the second phase of the formalin test, but not the first phase.[64] In contrast, stronger analgesics such as opioids block pain behaviors in both phases, in part, because they directly inhibit nociceptors which generate pain in Phase 1 and Phase 2.[64] Given that the second phase is largely mediated by inflammatory processes, the antinociceptive effect observed in Fig. 6B is presumably due to the drug's ability to block pro-inflammatory mechanisms via sEH inhibition such as the conversion of EETs to DHETs as opposed to directly inhibiting nociceptors.[66] Another contributor to the antinociceptive effects seen in Fig. 6B is the inhibition of FAAH. FAAH inhibition has been shown to inhibit pain on the Formalin Test[67, 68], and pharmacological inhibitors of FAAH such as URB937 have also attenuated pain on the Formalin Test.[69] Similarly, the pain relief produced by FAAH inhibition is present in Phase 2 of the Formalin Test.[69] The role of inhibiting FAAH in the antinociceptive effects of **3** needs to be further explored as intraplantar injection of formalin increases the expression of AEA in the periaqueductal gray, an important brain region for pain processing.[70] Since **3** is our lead compound, these studies provide initial proof-of-concept data to suggest that dual sEH/FAAH inhibition can produce pain relief. Further analysis of the contribution of sEH inhibition and FAAH inhibition and *in vivo* potency and efficacy compared to existing analgesics and other novel dual inhibitors is needed.

## - Conclusion

Herein, several dual sEH/FAAH inhibitors with potencies in low nanomolar range were successfully designed, synthesized, and biologically evaluated. Several important SAR observations were established which will further guide our follow-up design and synthesis. In addition, a new class of dual inhibitors possessing the 4-phenylthiazol moiety was identified. Docking experiments reveal important key interactions within the catalytic sites of both enzymes permitting the description of the chemical space for this set of dual inhibitors. Next, several important ADMET properties of dual inhibitors **6l-p** were evaluated *in silico* and they suggest that the new compounds have good drug properties. Finally, the antinociceptive effects of our most potent dual inhibitor reported previously, **3**, was evaluated using a rat model of acute inflammatory pain which revealed that the antinociception produced by **3** is comparable to ketoprofen, a traditional NSAID. Information obtained here will be helpful during the drug formulation and planning of future *in vivo* experiments, and it will help toward our long-term goal to develop novel non-opioid therapeutics for pain management.

## Material and methods

All solvents and reagents were obtained from Sigma–Aldrich, Matrix Scientific, TCI, and Acr s Organic and used without further purification. Analytical thin-layer chromatography (TLC) was performed on aluminum plates precoated with silica gel, also obtained from Sigma–Aldrich. Flash chromatography was carried out on Teledyne CombiFlash Rf+ system. Proton and carbon NMR spectra were recorded with a Bruker 400 MHz NMR spectrometer. Proton chemical shifts are reported relative to the residual solvent peak (chloroform = 7.26 ppm or dimethyl sulfoxide = 2.50 ppm) as follows: chemical shift (δ), proton ID, multiplicity (s = singlet, bs = broad singlet, d = doublet, bd = broad

doublet, dd = doublet of doublets, t = triplet, q = quartet, m = multiplet, integration, coupling constant(s) in Hz. Carbon chemical shifts are reported relative to the residual deuterated solvent signals (chloroform = 77.2 ppm, or dimethyl sulfoxide = 39.5 ppm). All compounds described were of > 95% purity. Purity was confirmed by high-resolution liquid chromatography mass spectrometer (ThermoFisher Scientific system). Elution was isocratic with water (30%, +0.1% formic acid) and acetonitrile (70%, +0.1% formic acid) at a flow rate of 0.4 mL/min. For compounds containing chlorine and/or bromine, $^{35}$Cl and $^{79}$Br isotopes were measured, respectively. Microwave reactions were carried out in a CEM 2.0 Discover microwave synthesizer. Melting points were measured with a MEL-TEMP II melting point apparatus and are reported uncorrected. Human recombinant FAAH enzyme (Item No. 100101183, Batch No. 0523867) and human recombinant sEH enzyme (Item No. 10011669) were obtained from Cayman Chemical. Fig. 1 was created with BioRender.com. Molecular modeling studies and docking experiments were performed using ICM Pro Molsoft software.

## Experimental

### Chemistry

**General procedure for the preparation of anilines 7l to 7p**—The mixture of 4-aminothiobenzamide (6.02 mmol) and corresponding 2-bromoacetophenone (6.02 mmol) were dissolved in isopropanol (25 ml; Scheme 1- inner box). The reaction was stirred at 60 °C for 2.5 hr. The reaction mixture was cooled to 0 °C, and the crude product was filtered and washed with an additional 2 ml cold isopropanol. The crude product (aniline) was used for the next step without further purification.

4-(4-phenylthiazol-2-yl)aniline (**7l**) was obtained as a dark green solid in the amount of 1.370 g (90% yield). $^1$H NMR (400 MHz; DMSO-$d_6$): δ 8.13 (d, $J$ = 3.5 Hz, 1H), 8.05–7.98 (m, 4H), 7.50–7.45 (m, 2H), 7.40–7.35 (m, 1H), 7.22 (d, $J$ = 8.5 Hz, 2H), 4.44 (bs, 2H).$^{13}$C NMR (101 MHz, DMSO-$d_6$): δ 167.0, 155.4, 134.4, 129.2, 128.6, 128.0, 126.5, 120.7, 114.4 ppm. HRMS-ESI+: calculated for $C_{15}H_{12}N_2S$ + H: 253.0799; Found: 253.0792.

4-(4-(4-fluorophenyl)thiazol-2-yl)aniline (**7m**) was obtained as a gray solid in the amount of 0.768 g (47% yield). $^1$H NMR (400 MHz; DMSO-$d_6$): δ 8.15 (s, 1H), 8.07 (dt, $J$ = 11.6, 8.1 Hz, 4H), 7.32 (q, $J$ = 8.8 Hz, 4H). $^{13}$C NMR (101 MHz, DMSO-$d_6$): δ 166.7, 163.73, 161.2, 154.4, 138.1, 131.0, 130.9, 130.1, 128.7, 128.6, 128.0, 122.1, 116.2, 116.0, 114.7 ppm. HRMS-ESI+: calculated for $C_{15}H_{11}FN_2S$ + H: 271.0705; Found: 271.0697.

4-(4-(4-chlorophenyl)thiazol-2-yl)aniline (**7n**) was obtained as a gray solid in the amount of 1.007 g (58% yield). $^1$H NMR (400 MHz; DMSO-$d_6$): δ 8.22 (s, 1H), 8.05 (dd, $J$ = 10.1, 8.7 Hz, 2H), 7.53 (d, $J$ = 8.8 Hz, 1H), 7.32 (d, $J$ = 8.5 Hz, 1H).$^{13}$C NMR (101 MHz, DMSO-$d_6$): δ 166.9, 154.2, 138.5, 133.2, 133.1, 129.8, 129.2, 128.2, 128.0, 121.8, 115.5. ppm. HRMS-ESI+: calculated for $C_{15}H_{11}ClN_2S$ + H: 287.0410; Found: 287.0403

4-(4-(*p*-tolyl)thiazol-2-yl)aniline (**7o**) was obtained as a white shiny solid in the amount of 1.52 g (95% yield). $^1$H NMR (400 MHz; DMSO-$d_6$): δ 8.07 (s, 1H), 8.03 (d, $J$ = 8.7 Hz, 2H), 7.93 (d, $J$ = 8.1 Hz, 2H), 7.31–7.27 (m, 4H), 2.35 (s, 3H). $^{13}$C NMR (101 MHz,

DMSO-$d_6$): δ 166.6, 155.5, 138.0, 131.7, 129.8, 128.0, 126.5, 121.6, 113.9, 21.3 ppm. HRMS-ESI+: calculated for $C_{16}H_{14}N_2S$ + H: 267.0956; Found: 267.0949.

4-(4-(4-methoxyphenyl)thiazol-2-yl)aniline (**7p**) was obtained as a gray solid in the amount of 0.982 g (57% yield). $^1$H NMR (400 MHz; DMSO-d$_6$): δ 8.04 (d, *J* = 8.7 Hz, 2H), 8.00–7.96 (m, 3H), 7.34 (d, *J* = 8.7 Hz, 2H), 7.03 (d, *J* = 9.0 Hz, 2H), 3.81 (s, 3H). $^{13}$C NMR (101 MHz, DMSO-d$_6$): δ 1656.4, 159.7, 155.4, 137.9, 130.3, 128.0, 127.9, 127.1, 122.1, 114.6, 112.9, 55.6 ppm. HRMS-ESI+: calculated for $C_{16}H_{14}N_2OS$ + H: 283.3690; Found: 283.0898.

**General procedure for the preparation of 6a to 6p**—2-chlorobenzenesulfonyl chloride (9.5 mmol), methyl isonipecotate (14.25 mmol) and N,N-diisopropylethylamine (28.5 mmol) were dissolved in anhydrous dichloromethane (20 mL) and were subjected to microwave irradiation at 80 °C for 20 min. After removal of the solvent under reduced pressure, the residue was re-dissolved in ethyl acetate (25 mL), the organic layer was washed twice with 1 N HCl (25 mL), then aqueous solution of saturated sodium bicarbonate (25 mL), brine (25 mL), and was then dried over anhydrous sodium sulfate, filtered and concentrated. The crude product, a yellowish oil, was purified by flash chromatography (1:4 ethyl acetate/hexane solvent system) and the final product **4** was obtained as a yellow oil. Saponification of this methyl ester was achieved via the following procedure: a stirred solution of **4** (2.2 g, 6.92 mmol) in tetrahydrofuran (25 mL) was treated with a 2 M aqueous solution of lithium hydroxide (2 mL) and the reaction was stirred overnight at room temperature. Following concentration in vacuo, water (15 mL) and ethyl acetate were added (50 mL). The mixture was then cooled to 0 °C and 1 N HCl was added dropwise, while stirring, until the reaction became acidic. The organic layer was separated, dried over anhydrous sodium sulfate, filtered, and concentrated. The crude product was recrystallized in diethyl ether, and **5** was obtained as a white solid (1.93 g, 91% yield). Next, 0.23 mmol of a carboxylic acid **5**, 0.575 mmol of 1-ethyl-3-(3-dimethylaminopropyl) carbodiimide (EDC), 0.46 mmol of corresponding aniline and a catalytic amount of 4-dimethylaminopyridine (DMAP) were dissolved in 20 mL anhydrous dichloromethane and subjected to microwave irradiation at 80 °C for 20 min. The solvent was removed under reduced pressure and the residue was dissolved in ethyl acetate (20 mL), washed twice with 1 N HCl (2×25 mL) and aqueous solution of saturated sodium bicarbonate (25 mL). The organic layer was separated, dried over anhydrous sodium sulfate, filtered, and concentrated. The crude product was purified by flash chromatography using 1:1 ethyl acetate/hexane solvent system and final compounds were obtained.

Methyl 1-((2-chlorophenyl)sulfonyl)piperidine-4-carboxylate (**4**) was obtained as an yellowish thick oil in the amount of 2.25 g (74% yield). $^1$H NMR (400 MHz; CDCl$_3$): δ 8.08–8.06 (m, 1H), 7.55–7.48 (m, 2H), 7.41 (ddd, *J* = 7.9, 7.0, 1.7 Hz, 1H), 3.80–3.75 (m, 2H), 3.68 (s, 3H), 2.93 (ddd, *J* = 13.2, 10.7, 2.7 Hz, 2H), 2.43 (dd, *J* = 9.3, 5.3 Hz, 1H), 1.98 (dd, *J* = 13.5, 3.9 Hz, 2H), 1.84–1.77 (m, 2H). $^{13}$C NMR (101 MHz, CDCl$_3$): δ 174.3, 136.4, 133.5, 132.2, 132.1, 132.0, 126.9, 51.8, 44.8, 40.1, 27.8 ppm. HRMS-ESI+: calculated for $C_{13}H_{16}ClNO_4S$ + H: 318.0567; Found: 318.0560.

1-((2-chlorophenyl)sulfonyl)piperidine-4-carboxylic acid (**5**) was obtained as a white solid in the amount of 1.93 g (91% yield). ^{1}H NMR (400 MHz; CDCl$_3$): δ 8.08–8.05 (m, 1H), 7.55–7.38 (m, 3H), 3.78 (dt, *J* = 13.1, 3.8 Hz, 2H), 2.93 (ddd, *J* = 13.1, 10.7, 2.6 Hz, 2H), 2.50–2.44 (m, 1H), 2.02–1.97 (m, 2H), 1.85–1.76 (m, 2H). ^{13}C NMR (101 MHz, CDCl$_3$): δ 180.1, 136.3, 133.6, 132.2, 132.1, 132.0, 126.9, 44.7, 39.9, 27.5 ppm. HRMS-ESI+: calculated for C$_{12}$H$_{14}$ClNO$_4$S + H: 304.0410; Found: 304.0403.

1-((2-chlorophenyl)sulfonyl)-*N*-phenylpiperidine-4-carboxamide (**6a**) was obtained as a white solid in the amount of 37 mg (43% yield): mp 126–128 °C. ^{1}H NMR (400 MHz; DMSO-d$_6$): δ 9.89 (s, 1H), 8.02–8.00 (m, 1H), 7.74–7.67 (m, 2H), 7.60–7.56 (m, 3H), 7.28 (dd, *J* = 8.5, 7.5 Hz, 2H), 7.04–7.00 (m, 1H), 3.78–3.75 (m, 2H), 2.82 (td, *J* = 12.4, 2.4 Hz, 2H), 2.51–2.46 (m, 1H), 1.88–1.84 (m, 2H), 1.65–1.55 (m, 2H). ^{13}C NMR (101 MHz, DMSO-d$_6$): δ 173.0, 139.6, 136.3, 134.9, 132.7, 131.9, 131.3, 129.0, 128.2, 123.5, 119.6, 45.2, 42.0, 28.5 ppm. HRMS-ESI+: calculated for C$_{18}$H$_{19}$N$_2$O$_3$SCl + H: 379.0883; Found: 379.0874.

1-((2-chlorophenyl)sulfonyl)-*N*-(4-fluorophenyl)piperidine-4-carboxamide (**6b**) was obtained as a white solid in the amount of 65 mg (72% yield): mp 172–174 °C. ^{1}H NMR (400 MHz; DMSO-d$_6$): δ 9.95 (s, 1H), 8.00 (d, *J* = 7.8 Hz, 1H), 7.70 (q, *J* = 9.4 Hz, 2H), 7.57 (t, *J* = 6.1 Hz, 3H), 7.12 (td, *J* = 8.3, 0.2 Hz, 2H), 3.77–3.74 (m, 2H), 2.86–2.79 (m, 2H), 1.87–1.84 (m, 2H), 1.64–1.58 (m, 2H). ^{13}C NMR (101 MHz, DMSO-d$_6$): δ 172.9, 159.5, 157.1, 136.3, 136.0, 135.9, 134.9, 132.7, 131.9, 131.3, 128.2, 121.3, 115.7, 115.5, 45.1, 42.0, 28.4 ppm. HRMS-ESI+: calculated for C$_{18}$H$_{18}$N$_2$O$_3$SClF+ H: 397.0789; Found: 397.0780.

*N*-(4-chlorophenyl)-1-((2-chlorophenyl)sulfonyl)piperidine-4-carboxamide (**6c**) was obtained as a white solid in the amount of 52 mg (55% yield): mp 177–180 °C. ^{1}H NMR (400 MHz; DMSO-d$_6$): δ 10.04 (s, 1H), 8.00 (ddd, *J* = 7.9, 1.6, 0.4 Hz, 1H), 7.74–7.67 (m, 2H), 7.63–7.56 (m, 3H), 7.35–7.32 (m, 2H), 3.77–3.74 (m, 2H), 2.83 (td, *J* = 12.4, 2.4 Hz, 2H), 2.50 (dt, *J* = 3.7, 1.8 Hz, 1H), 1.86 (dd, *J* = 13.2, 2.7 Hz, 2H), 1.64–1.55 (m, 2H). ^{13}C NMR (101 MHz, DMSO-d$_6$): δ 1723.1, 138.5, 136.3, 134.9, 132.7, 131.9, 131.3, 129.0, 128.2, 127.1, 121.1, 45.1, 42.0, 28.4 ppm. HRMS-ESI+: calculated for C$_{18}$H$_{18}$N$_2$O$_3$SCl$_2$+ H: 413.0493; Found: 413.0482.

*N*-(4-bromophenyl)-1-((2-chlorophenyl)sulfonyl)piperidine-4-carboxamide (**6d**) was obtained as a white solid in the amount of 81 mg (77% yield): mp 184–186 °C. ^{1}H NMR (400 MHz; DMSO-d$_6$): δ 10.05 (s, 1H), 8.02–7.99 (m, 1H), 7.73–7.67 (m, 2H), 7.60–7.54 (m, 3H), 7.47–7.45 (m, 2H), 3.77–3.73 (m, 2H), 2.82 (td, *J* = 12.4, 2.3 Hz, 2H), 2.50 (dt, *J* = 3.7, 1.8 Hz, 1H), 1.88–1.84 (m, 2H), 1.64–1.55 (m, 2H). ^{13}C NMR (101 MHz; DMSO): δ 173.2, 139.0, 136.3, 134.9, 132.8, 131.99, 131.92, 131.3, 128.3, 121.5, 115.1, 45.2, 42.1, 28.4 ppm. HRMS-ESI+: calculated for C$_{18}$H$_{18}$N$_2$O$_3$SClBr+ H: 456.9988; Found: 456.9979.

1-((2-chlorophenyl)sulfonyl)-*N*-(*p*-tolyl)piperidine-4-carboxamide (**6e**) was obtained as a white solid in the amount of 51 mg (57% yield): mp 151–154 °C. ^{1}H NMR (400 MHz; DMSO-d$_6$): δ 9.80 (s, 1H), 8.02–7.99 (m, 1H), 7.72–7.69 (m, 2H), 7.60–7.56 (m, 1H), 7.46–7.44 (m, 2H), 7.08 (d, *J* = 8.2 Hz, 2H), 3.76 (d, *J* = 12.7 Hz, 2H), 2.81 (td, *J* = 12.4, 2.4 Hz,

2H), 2.51–2.48 (m, 1H), 2.23 (s, 3H), 1.86–1.82 (m, 2H), 1.64–1.54 (m, 2H). $^{13}$C NMR (101 MHz; DMSO): δ 172.8, 137.1, 136.3, 134.9, 132.8, 132.0, 131.3, 129.5, 128.3, 119.6, 45.2, 42.0, 28.5, 20.9 ppm. HRMS-ESI+: calculated for $C_{19}H_{21}N_2O_3SCl$+ H: 393.1040; Found: 393.1029.

1-((2-chlorophenyl)sulfonyl)-*N*-(4-(thiazol-2-yl)phenyl)piperidine-4-carboxamide (**6f**) was obtained as a light gray solid in the amount of 78 mg (74% yield): mp 204–205 °C. $^1$H NMR (400 MHz; DMSO-d$_6$): δ 10.16 (s, 1H), 8.02–8.00 (m, 1H), 7.90–7.87 (m, 3H), 7.74–7.67 (m, 5H), 7.58 (ddd, *J* = 7.9, 7.1, 1.6 Hz, 1H), 3.77 (d, *J* = 12.8 Hz, 2H), 2.87–2.81 (m, 2H), 1.88 (dd, *J* = 13.4, 3.0 Hz, 2H), 1.67–1.56 (m, 2H). $^{13}$C NMR (101 MHz; DMSO): δ 173.4, 167.4, 144.1, 141.3, 136.4, 134.9, 132.8, 132.0, 131.4, 128.43, 128.30, 127.3, 120.1, 119.8, 45.2, 42.2, 28.5 ppm. HRMS-ESI+: calculated for $C_{21}H_{20}N_3O_3S_2Cl$+ H: 462.0713; Found: 462.0701.

1-((2-chlorophenyl)sulfonyl)-*N*-(4-(oxazol-2-yl)phenyl)piperidine-4-carboxamide (**6g**) was obtained as a dark yellow solid in the amount of 93 mg (91% yield): mp 229–231 °C. $^1$H NMR (400 MHz; DMSO-d$_6$): δ 10.19 (s, 1H), 8.16 (d, *J* = 0.8 Hz, 1H), 8.02–8.00 (m, 1H), 7.92–7.90 (m, 2H), 7.76–7.69 (m, 4H), 7.60–7.58 (m, 1H), 7.33 (d, *J* = 0.8 Hz, 1H), 3.79–3.76 (m, 2H), 2.87–2.81 (m, 2H), 1.90–1.86 (m, 2H), 1.66–1.56 (m, 2H). $^{13}$C NMR (101 MHz; DMSO): δ 173.4, 161.2, 141.6, 140.1, 136.3, 134.9, 132.8, 132.0, 131.3, 128.8, 128.3, 127.1, 122.2, 119.7, 45.2, 42.2, 28.5 ppm. HRMS-ESI+: calculated for $C_{21}H_{20}N_3O_4SCl$+ H: 446.0941; Found: 446.0941.

1-((2-chlorophenyl)sulfonyl)-*N*-(4-(5-methylbenzo[*d*]thiazol-2-yl)phenyl)piperidine-4-carboxamide (**6h**) was obtained as a white solid in the amount of 63 mg (52% yield): mp >250 °C. $^1$H-NMR (400 MHz; DMSO-d$_6$): δ 10.24 (s, 1H), 8.03–7.99 (m, 3H), 7.90–7.88 (m, 2H), 7.79–7.67 (m, 4H), 7.58 (ddd, *J* = 7.9, 7.1, 1.6 Hz, 1H), 7.34 (ddd, *J* = 8.4, 1.7, 0.6 Hz, 1H), 3.78 (d, *J* = 12.7 Hz, 2H), 2.87–2.82 (m, 2H), 2.45 (s, 3H), 1.91–1.87 (m, 2H), 1.67–1.58 (m, 2H). $^{13}$C NMR (101 MHz; DMSO): δ 173.5, 166.3, 152.2, 142.3, 136.3, 135.5, 134.95, 134.86, 132.8, 132.0, 131.4, 128.47, 128.30, 128.25, 128.11, 122.6, 122.2, 119.8, 45.2, 42.2, 28.5, 21.5 ppm. HRMS-ESI+: calculated for $C_{26}H_{24}N_3O_3S_2Cl$+ H: 526.1026; Found: 526.1014.

1-((2-chlorophenyl)sulfonyl)-*N*-(4-(1-methyl-1*H*-benzo[*d*]imidazol-2-yl)phenyl)piperidine-4-carboxamide (**6i**) was obtained as a light gray solid in the amount of 80 mg (68% yield): mp 195–198 °C. $^1$H NMR (400 MHz; DMSO-d$_6$): δ 10.19 (s, 1H), 8.02 (dd, *J* = 7.8, 1.4 Hz, 1H), 7.80 (s, 4H), 7.74–7.64 (m, 3H), 7.61–7.57 (m, 2H), 7.25 (dtd, *J* = 19.3, 7.5, 1.3 Hz, 2H), 3.87 (s, 3H), 3.79 (d, *J* = 12.7 Hz, 2H), 2.88–2.82 (m, 2H), 2.50 (s, 1H), 1.92–1.88 (m, 2H), 1.69–1.60 (m, 2H). $^{13}$C NMR (101 MHz; DMSO): δ 173.4, 172.5, 153.28, 153.24, 152.8, 144.4, 142.9, 140.8, 137.1, 136.4, 135.0, 132.77, 132.68, 132.0, 131.4, 130.3, 129.5, 128.3, 125.1, 122.6, 122.3, 122.0, 121.0, 119.36, 119.25, 116.2, 114.0, 113.8, 110.9, 109.3, 107.5, 45.2, 42.2, 32.2, 28.5 ppm. HRMS-ESI+: calculated for $C_{26}H_{25}N_4O_3SCl$+ H: 509.1414; Found: 509.1400.

*N*-(4-(benzo[*d*][1,3]oxathiol-2-yl)phenyl)-1-((2-chlorophenyl)sulfonyl)piperidine-4-carboxamide (**6j**) was obtained as a gray solid in the amount of 28 mg (24% yield):

mp 221–224 °C. ^{1}H NMR (400 MHz; DMSO-d$_6$): δ 10.31 (s, 1H), 8.15–8.12 (m, 2H), 8.03–8.00 (m, 1H), 7.84–7.67 (m, 6H), 7.58 (ddd, $J$ = 7.9, 7.1, 1.6 Hz, 1H), 7.42–7.38 (m, 2H), 3.78 (d, $J$ = 12.7 Hz, 2H), 2.88–2.82 (m, 2H), 2.54 (s, 1H), 1.92–1.88 (m, 2H), 1.68–1.58 (m, 2H). ^{13}C NMR (101 MHz; DMSO): δ 173.6, 162.7, 150.6, 142.9, 142.1, 136.4, 135.0, 132.8, 132.0, 131.4, 128.7, 128.3, 125.6, 125.2, 121.2, 120.0, 119.7, 111.2, 45.2, 42.2, 28.4 ppm. HRMS-ESI+: calculated for $C_{25}H_{23}N_2O_4S_2Cl$+ H: 515.0866; Found: 515.0860.

*N*-(4-(4-chlorobenzyl)phenyl)-1-((2-chlorophenyl)sulfonyl)piperidine-4-carboxamide (**6k**) was obtained as a white solid in the amount of 69 mg (70% yield): mp 135–136 °C. ^{1}H NMR (400 MHz; DMSO-d$_6$): δ 8.37 (t, $J$ = 6.0 Hz, 1H), 8.00–7.97 (m, 1H), 7.72–7.65 (m, 2H), 7.57 (ddd, $J$ = 7.9, 6.9, 1.8 Hz, 1H), 7.38–7.34 (m, 2H), 7.24–7.21 (m, 2H), 4.22 (d, $J$ = 6.0 Hz, 2H), 3.72–3.69 (m, 2H), 2.79 (td, $J$ = 12.3, 2.4 Hz, 2H), 2.35–2.29 (m, 1H), 1.78 (dd, $J$ = 13.3, 3.0 Hz, 2H), 1.59–1.49 (m, 2H). ^{13}C NMR (101 MHz; DMSO): δ 174.0, 139.1, 136.3, 134.9, 132.7, 132.0, 131.7, 131.3, 129.4, 128.7, 128.3, 45.2, 41.7, 41.1, 28.6 ppm. HRMS-ESI+: calculated for $C_{25}H_{24}N_2O_3SCl_2$+ H: 503.0963; Found: 503.0954.

1-((2-chlorophenyl)sulfonyl)-N-(4-(4-phenylthiazol-2-yl)phenyl)piperidine-4-carboxamide (**6l**) was obtained as an off-white solid in the amount of 55 mg (44% yield): mp 172–174 °C. ^{1}H NMR (400 MHz; DMSO-d$_6$): δ 10.19 (s, 1H), 8.11 (s, 1H), 8.06–7.96 (m, 5H), 7.77–7.67 (m, 4H), 7.59 (ddd, $J$ = 7.9, 7.1, 1.6 Hz, 1H), 7.50–7.46 (m, 2H), 7.39–7.35 (m, 1H), 3.78 (d, $J$ = 12.8 Hz, 2H), 2.85 (td, $J$ = 12.3, 2.2 Hz, 2H), 1.89 (dd, $J$ = 13.4, 2.8 Hz, 2H), 1.66–1.58 (m, 2H). ^{13}C NMR (101 MHz; DMSO): δ 173.4, 167.2, 155.4, 141.5, 136.4, 134.9, 134.5, 132.8, 132.0, 131.4, 129.3, 128.6, 128.3, 127.3, 126.6, 119.8, 114.3, 100.1, 45.2, 42.2, 28.5 ppm. HRMS-ESI+: calculated for $C_{27}H_{24}ClN_3O_3S_2$+ H: 538.1020; Found: 538.1007.

1-((2-chlorophenyl)sulfonyl)-N-(4-(4-(4-fluorophenyl)thiazol-2-yl)phenyl)piperidine-4-carboxamide (**6m**) was obtained as a pale yellow solid in the amount 57 mg (45%): mp 182–185 °C. ^{1}H NMR (400 MHz; DMSO-d$_6$): δ 10.18 (s, 1H), 8.10–8.06 (m, 3H), 8.02–7.95 (m, 3H), 7.76–7.67 (m, 4H), 7.58 (ddd, $J$ = 7.9, 7.1, 1.6 Hz, 1H), 7.31 (dd, $J$ = 10.0, 7.9 Hz, 2H), 3.78 (d, $J$ = 12.7 Hz, 2H), 2.84 (td, $J$ = 12.3, 2.2 Hz, 2H), 1.91–1.87 (m, 2H), 1.67–1.57 (m, 2H). ^{13}C NMR (101 MHz, DMSO-d$_6$): δ 173.4, 167.3, 154.4, 141.6, 136.56, 136.37, 134.9, 132.8, 132.0, 131.4, 128.68, 128.60, 128.30, 128.20, 127.3, 119.8, 116.2, 116.0, 114.1, 45.2, 42.2, 28.5 ppm. HRMS-ESI+: calculated for $C_{27}H_{23}ClFN_3O_3S_2$+ H: 556.0932; Found 556.0919.

1-((2-chlorophenyl)sulfonyl)-N-(4-(4-(4-chlorophenyl)thiazol-2-yl)phenyl)piperidine-4-carboxamide (**6n**) was obtained as an off-white solid in the amount of 61 mg (46% yield): mp 188–190 °C. ^{1}H NMR (400 MHz, DMSO-d$_6$) δ 10.20 (s, 1H), 8.17 (s, 1H), 8.07–7.95 (m, 5H), 7.76–7.69 (m, 4H), 7.58–7.52 (m, 3H), 3.79–3.75 (m, 2H), 2.87–2.81 (m, 2H), 1.91–1.87 (m, 2H), 1.63–1.59 (m, 2H). ^{13}C NMR (100 MHz, DMSO-d$_6$): δ 173.4, 167.4, 154.1, 141.6, 136.4, 134.9, 133.3, 133.1, 132.8, 132.0, 131.3, 129.3, 128.28, 128.14, 127.3, 119.8, 115.1, 100.0, 45.2, 42.2, 28.5 ppm. HRMS-ESI+: calculated for $C_{27}H_{23}Cl_2N_3O_3S_2$+ H: 572.0636; Found 572.0626.

1-((2-chlorophenyl)sulfonyl)-N-(4-(4-(p-tolyl)thiazol-2-yl)phenyl)piperidine-4-carboxamide (**6o**) was obtained as a white solid in the amount of 65 mg (52% yield): mp 230–233 °C. ^{1}H NMR (400 MHz; DMSO-$d_6$): δ 10.18 (s, 1H), 8.03–8.00 (m, 2H), 7.97–7.92 (m, 4H), 7.76–7.69 (m, 4H), 7.58 (ddd, $J$ = 7.9, 7.1, 1.6 Hz, 1H), 7.28 (dd, $J$ = 8.5, 0.6 Hz, 2H), 3.78 (dd, $J$ = 12.6, 0.3 Hz, 2H), 2.88–2.81 (m, 2H), 2.35 (s, 3H), 1.91–1.87 (m, 2H), 1.67–1.57 (m, 2H). ^{13}C NMR (100 MHz, DMSO-$d_6$): δ 173.4, 167.0, 156.6, 155.5, 141.5, 138.0, 136.4, 134.9, 132.8, 132.00, 131.84, 131.4, 129.8, 128.36, 128.30, 127.3, 126.5, 119.8, 113.5, 45.2, 42.2, 28.5, 21.3 ppm. HRMS-ESI+: calculated for $C_{28}H_{26}ClN_3O_3S_2$+ H: 552.1182; Found: 552.1170.

1-((2-chlorophenyl)sulfonyl)-N-(4-(4-(4-methoxyphenyl)thiazol-2-yl)phenyl)piperidine-4-carboxamide (**6p**) was obtained as an off-white solid in the amount of 68 mg (52% yield): mp 207–209 °C. ^{1}H NMR (400 MHz; DMSO-$d_6$): δ 10.17 (s, 1H), 8.03–7.93 (m, 6H), 7.75–7.69 (m, 4H), 7.60–7.57 (m, 1H), 7.03 (d, $J$ = 9.0 Hz, 2H), 3.81 (d, $J$ = 6.2 Hz, 3H), 3.78 (d, $J$ = 12.9 Hz, 2H), 2.87–2.81 (m, 2H), 1.91–1.87 (m, 2H), 1.66–1.60 (m, 2H).. ^{13}C NMR (101 MHz; DMSO): δ 173.4, 167.0, 159.7, 155.4, 141.4, 136.4, 134.9, 132.8, 132.0, 131.4, 128.40, 128.30, 127.9, 127.34, 127.24, 119.8, 114.6, 112.3, 55.7, 45.2, 42.2, 28.5 ppm. HRMS-ESI+: calculated for $C_{28}H_{26}ClN_3O_4S_2$+ H: 568.1132; Found 568.1119.

### Biological evaluation

Experimental details for the quantification of inhibitor potencies have been previously published for both FAAH and sEH enzymes.[32] In brief, fluorescence generated by hydrolysis was quantified every 30 seconds for 10 minutes and the linear portion of the curve was used to generate the reaction velocity ($v_{inhibitor}$). Values were subtracted from wells containing no enzyme. Next, the $IC_{50}$ values were quantified by simple linear regression of the log [I] vs. % remaining activity ($v_{inhibitor}/v_{DMSO}$) and determining x when y = 0.50. All measurements were the average of triplicates. For all assays, the final DMSO concentration was 2%.

**sEH Assay.**—The substrate cyano(6-methoxynaphthalen-2-yl)methyl((3-phenyloxiran-2-yl)methyl)carbonate (CMNPC) ($[S]_{final}$ = 5 μM) was added to wells containing human sEH in sodium phosphate buffer [0.1 M, pH = 7.4 and 0.1 mg/mL bovine serum albumin (BSA)], and formation of the fluorescent 6-methoxynaphthaldehyde ($\lambda_{excitation}$ = 330 nm, $\lambda_{emission}$ = 465 nm, 30 °C) was measured by the use of a microplate reader (Molecular Devices., CA, USA).

**FAAH Assay.**—Measurement of human FAAH potency was performed using the substrate N-(6-methoxypyridin-3-yl) octanamide (OMP) ($[S]_{final}$ = 50 μM) in sodium phosphate buffer (0.1 M, pH = 8, 0.1 mg/mL BSA). Progress of the reaction was measured by fluorescence detection of 6-methoxypyridin-3-amine at an excitation wavelength of 303 nm and an emission wavelength of 394 nm at 37 °C by the use of a microplate reader (Molecular Devices., CA, USA). The substrate, OMP, was synthesized following a previously reported synthetic procedure and reaction conditions.[37]

## Molecular modeling

For the docking studies of the dual sEH/FAAH inhibitors, a crystal structure of human soluble epoxide hydrolase complexed with N-cycloheptyl-1-(mesitylsulfonyl)piperidine-4-carboxamide (PDBfile: 4HAI)[33] and a homology model of human FAAH enzyme[37] were used. The PDB file 4HAI was first converted to an ICM file and the inhibitor, *N*-cycloheptyl-1-(mesitylsulfonyl) piperidine-4-carboxamide, was removed. Docking experiments were performed following the program guidelines. ICM scores were obtained after this procedure. ADMET properties for all synthesized target analogs were calculated using the ICM Chemist Pro program. To generate a Consensus Pharmacophore based on the Atomic Property Fields[71] the following steps were executed according to the program guidelines: (i) dual inhibitors 6l-p were first converted into an ICM objects; (ii) using APF fields, the dual inhibitors **6l-p** were superimposed based on substructures; (iii) the ligands were selected and Choose the Consensus Ph4 menu option was applied; (iv) the threshold was selected as 0.90 (the pharmacophore will be displayed if the property is found in 90% or more of the ligands). The consensus is displayed as meshes in Fig. 5.

## Behavior

**Subjects:** Data were collected from male Sprague-Dawley rats purchased from Charles River (Hollister, CA, USA) and housed at California State University, East Bay (Hayward, CA, USA). All rats were at least 50 days old at the start of the study and randomly assigned to treatment groups. Experimenters were blinded to treatment groups. Procedures were approved by the Institutional Animal Care and Use Committee of California State University, East Bay.

**Drugs: 3** was dissolved in DMSO to a stock concentration of 10 mM. The 10 mM stock was further diluted into injectable doses (0.1 and 1.0 mg/kg) using a vehicle solution comprising 10% ethanol, 10% cremophor, and 80% saline. Ketoprofen (Sigma-Aldrich, St. Louis, MO, USA) was dissolved in the same vehicle. Drugs were injected intraperitoneally in a volume of 1 mL/kg. All drugs were administered 30 min before hindpaw injection of formalin.

**Formalin Test:** The Formalin Test is a common test of acute inflammatory pain. Rats were removed from their home cages and briefly anesthetized with isoflurane. A dilute formalin solution (5%, 50 μL) was then injected into the plantar surface of the right hindpaw. Rats were placed on an elevated mesh rack for observation. The amount of time spent licking or guarding the injected hindpaw was measured in seconds in 5 min blocks for one hour following hindpaw injection.

**Statistical Analysis:** All data are expressed as mean ± SEM. A one-way analysis of variance (ANOVA) followed by a Tukey post-hoc test was used to evaluate differences between groups. Statistical significance was defined as a probability of $< 0.05$.

## Supplementary Material

Refer to Web version on PubMed Central for supplementary material.

## Acknowledgments

## References

1. Russo CM; Brose WG, Chronic pain. Annu Rev Med 1998, 49, 123–33. [PubMed: 9509254]

2. Smith BH; Elliott AM; Chambers WA; Smith WC; Hannaford PC; Penny K, The impact of chronic pain in the community. Fam Pract 2001, 18 (3), 292–9. [PubMed: 11356737]

3. Chen L; Deng H; Cui H; Fang J; Zuo Z; Deng J; Li Y; Wang X; Zhao L, Inflammatory responses and inflammation-associated diseases in organs. Oncotarget 2018, 9 (6), 7204–7218. [PubMed: 29467962]

4. Zhou Y; Hong Y; Huang H, Triptolide Attenuates Inflammatory Response in Membranous Glomerulo-Nephritis Rat via Downregulation of NF-κB Signaling Pathway. Kidney Blood Press Res 2016, 41 (6), 901–910. [PubMed: 27871079]

5. Marchand F; Perretti M; McMahon SB, Role of the immune system in chronic pain. Nat Rev Neurosci 2005, 6 (7), 521–32. [PubMed: 15995723]

6. Ren K; Dubner R, Interactions between the immune and nervous systems in pain. Nat Med 2010, 16 (11), 1267–76. [PubMed: 20948535]

7. Rainsford KD, Profile and mechanisms of gastrointestinal and other side effects of nonsteroidal anti-inflammatory drugs (NSAIDs). Am J Med 1999, 107 (6A), 27S–35S; discussion 35S-36S.

8. Diaz-Gonzalez F; Sanchez-Madrid F, NSAIDs: learning new tricks from old drugs. Eur J Immunol 2015, 45 (3), 679–86. [PubMed: 25523026]

9. Imig JD; Hammock BD, Soluble epoxide hydrolase as a therapeutic target for cardiovascular diseases. Nat Rev Drug Discov 2009, 8 (10), 794–805. [PubMed: 19794443]

10. Morisseau C; Hammock BD, Impact of soluble epoxide hydrolase and epoxyeicosanoids on human health. Annu Rev Pharmacol Toxicol 2013, 53, 37–58. [PubMed: 23020295]

11. Harris TR; Hammock BD, Soluble epoxide hydrolase: gene structure, expression and deletion. Gene 2013, 526 (2), 61–74. [PubMed: 23701967]

12. Enayetallah AE; French RA; Thibodeau MS; Grant DF, Distribution of soluble epoxide hydrolase and of cytochrome P450 2C8, 2C9, and 2J2 in human tissues. J Histochem Cytochem 2004, 52 (4), 447–54. [PubMed: 15033996]

13. Lillich FF; Imig JD; Proschak E, Multi-Target Approaches in Metabolic Syndrome. Front Pharmacol 2020, 11, 554961. [PubMed: 33776749]

14. Kodani SD; Morisseau C, Role of epoxy-fatty acids and epoxide hydrolases in the pathology of neuro-inflammation. Biochimie 2019, 159, 59–65. [PubMed: 30716359]

15. Schmelzer KR; Kubala L; Newman JW; Kim IH; Eiserich JP; Hammock BD, Soluble epoxide hydrolase is a therapeutic target for acute inflammation. Proc Natl Acad Sci U S A 2005, 102 (28), 9772–7. [PubMed: 15994227]

16. Wagner KM; McReynolds CB; Schmidt WK; Hammock BD, Soluble epoxide hydrolase as a therapeutic target for pain, inflammatory and neurodegenerative diseases. Pharmacol Ther 2017, 180, 62–76. [PubMed: 28642117]

17. Pillarisetti S; Khanna I, A multimodal disease modifying approach to treat neuropathic pain-- inhibition of soluble epoxide hydrolase (sEH). Drug Discov Today 2015, 20 (11), 1382–90. [PubMed: 26259523]

18. Inceoglu B; Jinks SL; Schmelzer KR; Waite T; Kim IH; Hammock BD, Inhibition of soluble epoxide hydrolase reduces LPS-induced thermal hyperalgesia and mechanical allodynia in a rat model of inflammatory pain. Life Sci 2006, 79 (24), 2311–9. [PubMed: 16962614]

19. Cravatt BF; Lichtman AH, Fatty acid amide hydrolase: an emerging therapeutic target in the endocannabinoid system. Curr Opin Chem Biol 2003, 7 (4), 469–75. [PubMed: 12941421]

20. McKinney MK; Cravatt BF, Structure and function of fatty acid amide hydrolase. Annu Rev Biochem 2005, 74, 411–32. [PubMed: 15952893]

21. Clayton N; Marshall FH; Bountra C; O'Shaughnessy CT, CB1 and CB2 cannabinoid receptors are implicated in inflammatory pain. Pain 2002, 96 (3), 253–260. [PubMed: 11972997]

22. Gauthier KM; Baewer DV; Hittner S; Hillard CJ; Nithipatikom K; Reddy DS; Falck JR; Campbell WB, Endothelium-derived 2-arachidonylglycerol: an intermediate in vasodilatory eicosanoid release in bovine coronary arteries. Am J Physiol Heart Circ Physiol 2005, 288 (3), H1344–51. [PubMed: 15528233]

23. Iliff JJ; Jia J; Nelson J; Goyagi T; Klaus J; Alkayed NJ, Epoxyeicosanoid signaling in CNS function and disease. Prostaglandins Other Lipid Mediat 2010, 91 (3–4), 68–84. [PubMed: 19545642]

24. Huggins JP; Smart TS; Langman S; Taylor L; Young T, An efficient randomised, placebo-controlled clinical trial with the irreversible fatty acid amide hydrolase-1 inhibitor PF-04457845, which modulates endocannabinoids but fails to induce effective analgesia in patients with pain due to osteoarthritis of the knee. Pain 2012, 153 (9), 1837–1846. [PubMed: 22727500]

25. Snider NT; Nast JA; Tesmer LA; Hollenberg PF, A cytochrome P450-derived epoxygenated metabolite of anandamide is a potent cannabinoid receptor 2-selective agonist. Mol Pharmacol 2009, 75 (4), 965–72. [PubMed: 19171674]

26. McDougle DR; Watson JE; Abdeen AA; Adili R; Caputo MP; Krapf JE; Johnson RW; Kilian KA; Holinstat M; Das A, Anti-inflammatory ω−3 endocannabinoid epoxides. Proc Natl Acad Sci U S A 2017, 114 (30), E6034–e6043. [PubMed: 28687674]

27. Sasso O; Wagner K; Morisseau C; Inceoglu B; Hammock BD; Piomelli D, Peripheral FAAH and soluble epoxide hydrolase inhibitors are synergistically antinociceptive. Pharmacol Res 2015, 97, 7–15. [PubMed: 25882247]

28. Proschak E; Stark H; Merk D, Polypharmacology by Design: A Medicinal Chemist's Perspective on Multitargeting Compounds. J Med Chem 2019, 62 (2), 420–444. [PubMed: 30035545]

29. Morphy R; Kay C; Rankovic Z, From magic bullets to designed multiple ligands. Drug Discov Today 2004, 9 (15), 641–51. [PubMed: 15279847]

30. Palermo G; Favia AD; Convertino M; De Vivo M, The Molecular Basis for Dual Fatty Acid Amide Hydrolase (FAAH)/Cyclooxygenase (COX) Inhibition. ChemMedChem 2016, 11 (12), 1252–1258. [PubMed: 26593700]

31. Abdelazeem AH; Safi El-Din AG; Abdel-Fattah MM; Amin NH; El-Moghazy SM; El-Saadi MT, Discovery of novel urea-diarylpyrazole hybrids as dual COX-2/sEH inhibitors with improved anti-inflammatory activity and highly reduced cardiovascular risks. European Journal of Medicinal Chemistry 2020, 205, 112662. [PubMed: 32763463]

32. Wilt S; Kodani S; Le TNH; Nguyen L; Vo N; Ly T; Rodriguez M; Hudson PK; Morisseau C; Hammock BD; Pecic S, Development of multitarget inhibitors for the treatment of pain: Design, synthesis, biological evaluation and molecular modeling studies. Bioorg Chem 2020, 103, 104165. [PubMed: 32891856]

33. Pecic S; Pakhomova S; Newcomer ME; Morisseau C; Hammock BD; Zhu Z; Rinderspacher A; Deng S-X, Synthesis and structure–activity relationship of piperidine-derived non-urea soluble epoxide hydrolase inhibitors. Bioorganic & Medicinal Chemistry Letters 2013, 23 (2), 417–421. [PubMed: 23237835]

34. Pecic S; Deng SX; Morisseau C; Hammock BD; Landry DW, Design, synthesis and evaluation of non-urea inhibitors of soluble epoxide hydrolase. Bioorg Med Chem Lett 2012, 22 (1), 601–5. [PubMed: 22079754]

35. Takebe T; Imai R; Ono S, The Current Status of Drug Discovery and Development as Originated in United States Academia: The Influence of Industrial and Academic Collaboration on Drug Discovery and Development. Clin Transl Sci 2018, 11 (6), 597–606. [PubMed: 29940695]

36. Dowden H; Munro J, Trends in clinical success rates and therapeutic focus. Nat Rev Drug Discov 2019, 18 (7), 495–496. [PubMed: 31267067]

37. Wilt SR; Rodriguez M; Le TNH; Baltodano EV; Salas A; Pecic S, Design, microwave-assisted synthesis, biological evaluation and molecular modeling studies of 4-phenylthiazoles as potent fatty acid amide hydrolase inhibitors. Chem Biol Drug Des 2020, 95 (5), 534–547. [PubMed: 32061147]

38. Wang X; Sarris K; Kage K; Zhang D; Brown SP; Kolasa T; Surowy C; El Kouhen OF; Muchmore SW; Brioni JD; Stewart AO, Synthesis and evaluation of benzothiazole-based analogues as novel, potent, and selective fatty acid amide hydrolase inhibitors. J Med Chem 2009, 52 (1), 170–80. [PubMed: 19072118]

39. Pecic S; Zeki AA; Xu X; Jin GY; Zhang S; Kodani S; Halim M; Morisseau C; Hammock BD; Deng SX, Novel piperidine-derived amide sEH inhibitors as mediators of lipid metabolism with improved stability. Prostaglandins Other Lipid Mediat 2018, 136, 90–95. [PubMed: 29567338]

40. Otrubova K; Ezzili C; Boger DL, The discovery and development of inhibitors of fatty acid amide hydrolase (FAAH). Bioorganic & Medicinal Chemistry Letters 2011, 21 (16), 4674–4685. [PubMed: 21764305]

41. Keith JM; Jones W; Pierce JM; Seierstad M; Palmer JA; Webb M; Karbarz M; Scott BP; Wilson SJ; Luo L; Wennerholm M; Chang L; Rizzolio M; Rynberg R; Chaplan S; Guy Breitenbucher J, Heteroarylureas with fused bicyclic diamine cores as inhibitors of fatty acid amide hydrolase. Bioorganic & Medicinal Chemistry Letters 2020, 30 (20), 127463. [PubMed: 32784090]

42. Ahn K; Johnson DS; Mileni M; Beidler D; Long JZ; McKinney MK; Weerapana E; Sadagopan N; Liimatta M; Smith SE; Lazerwith S; Stiff C; Kamtekar S; Bhattacharya K; Zhang Y; Swaney S; Van Becelaere K; Stevens RC; Cravatt BF, Discovery and characterization of a highly selective FAAH inhibitor that reduces inflammatory pain. Chem Biol 2009, 16 (4), 411–20. [PubMed: 19389627]

43. Kodani SD; Bhakta S; Hwang SH; Pakhomova S; Newcomer ME; Morisseau C; Hammock BD, Identification and optimization of soluble epoxide hydrolase inhibitors with dual potency towards fatty acid amide hydrolase. Bioorganic & Medicinal Chemistry Letters 2018, 28 (4), 762–768. [PubMed: 29366648]

44. Jones PD; Wolf NM; Morisseau C; Whetstone P; Hock B; Hammock BD, Fluorescent substrates for soluble epoxide hydrolase and application to inhibition studies. Analytical Biochemistry 2005, 343 (1), 66–75. [PubMed: 15963942]

45. Hwang SH; Tsai HJ; Liu JY; Morisseau C; Hammock BD, Orally bioavailable potent soluble epoxide hydrolase inhibitors. J Med Chem 2007, 50 (16), 3825–40. [PubMed: 17616115]

46. Kodani SD; Wan D; Wagner KM; Hwang SH; Morisseau C; Hammock BD, Design and Potency of Dual Soluble Epoxide Hydrolase/Fatty Acid Amide Hydrolase Inhibitors. ACS Omega 2018, 3 (10), 14076–14086. [PubMed: 30411058]

47. Xu W; Lucke AJ; Fairlie DP, Comparing sixteen scoring functions for predicting biological activities of ligands for protein targets. Journal of Molecular Graphics and Modelling 2015, 57, 76–88. [PubMed: 25682361]

48. Li Y; Su M; Liu Z; Li J; Liu J; Han L; Wang R, Assessing protein–ligand interaction scoring functions with the CASF-2013 benchmark. Nature Protocols 2018, 13 (4), 666–680. [PubMed: 29517771]

49. Abagyan R; Totrov M, Biased probability Monte Carlo conformational searches and electrostatic calculations for peptides and proteins. J Mol Biol 1994, 235 (3), 983–1002. [PubMed: 8289329]

50. Lam PCH; Abagyan R; Totrov M, Hybrid receptor structure/ligand-based docking and activity prediction in ICM: development and evaluation in D3R Grand Challenge 3. Journal of Computer-Aided Molecular Design 2019, 33 (1), 35–46. [PubMed: 30094533]

51. Lam PCH; Abagyan R; Totrov M, Ligand-biased ensemble receptor docking (LigBEnD): a hybrid ligand/receptor structure-based approach. Journal of Computer-Aided Molecular Design 2018, 32 (1), 187–198. [PubMed: 28887659]

52. Scarpino A; Ferenczy GG; Keser GM, Comparative Evaluation of Covalent Docking Tools. Journal of Chemical Information and Modeling 2018, 58 (7), 1441–1458. [PubMed: 29890081]

53. Mileni M; Kamtekar S; Wood DC; Benson TE; Cravatt BF; Stevens RC, Crystal Structure of Fatty Acid Amide Hydrolase Bound to the Carbamate Inhibitor URB597: Discovery of a Deacylating

Water Molecule and Insight into Enzyme Inactivation. Journal of Molecular Biology 2010, 400 (4), 743–754. [PubMed: 20493882]

54. Ahn K; Johnson DS; Cravatt BF, Fatty acid amide hydrolase as a potential therapeutic target for the treatment of pain and CNS disorders. Expert Opin Drug Discov 2009, 4 (7), 763–784. [PubMed: 20544003]

55. Lipinski CA, Drug-like properties and the causes of poor solubility and poor permeability. J Pharmacol Toxicol Methods 2000, 44 (1), 235–49. [PubMed: 11274893]

56. Lipinski CA; Lombardo F; Dominy BW; Feeney PJ, Experimental and computational approaches to estimate solubility and permeability in drug discovery and development settings. Adv Drug Deliv Rev 2001, 46 (1–3), 3–26. [PubMed: 11259830]

57. Veber DF; Johnson SR; Cheng HY; Smith BR; Ward KW; Kopple KD, Molecular properties that influence the oral bioavailability of drug candidates. J Med Chem 2002, 45 (12), 2615–23. [PubMed: 12036371]

58. Benet LZ; Hosey CM; Ursu O; Oprea TI, BDDCS, the Rule of 5 and drugability. Adv Drug Deliv Rev 2016, 101, 89–98. [PubMed: 27182629]

59. van Breemen RB; Li Y, Caco-2 cell permeability assays to measure drug absorption. Expert Opin Drug Metab Toxicol 2005, 1 (2), 175–85. [PubMed: 16922635]

60. Inanobe A; Kamiya N; Murakami S; Fukunishi Y; Nakamura H; Kurachi Y, In silico prediction of the chemical block of human ether-a-go-go-related gene (hERG) K+ current. J Physiol Sci 2008, 58 (7), 459–70. [PubMed: 19032804]

61. Braga RC; Alves VM; Silva MF; Muratov E; Fourches D; Tropsha A; Andrade CH, Tuning HERG out: antitarget QSAR models for drug development. Curr Top Med Chem 2014, 14 (11), 1399–415. [PubMed: 24805060]

62. Banerjee P; Eckert AO; Schrey AK; Preissner R, ProTox-II: a webserver for the prediction of toxicity of chemicals. Nucleic Acids Research 2018, 46 (W1), W257–W263. [PubMed: 29718510]

63. Dubuisson D; Dennis SG, The formalin test: a quantitative study of the analgesic effects of morphine, meperidine, and brain stem stimulation in rats and cats. Pain 1977, 4 (2), 161–174. [PubMed: 564014]

64. Hunskaar S; Hole K, The formalin test in mice: dissociation between inflammatory and non-inflammatory pain. Pain 1987, 30 (1), 103–114. [PubMed: 3614974]

65. Jourdan D; Ardid D; Bardin L; Bardin M; Neuzeret D; Lanphouthacoul L; Eschalier A, A new automated method of pain scoring in the formalin test in rats. Pain 1997, 71 (3), 265–270. [PubMed: 9231869]

66. Wang Y; Wagner KM; Morisseau C; Hammock BD, Inhibition of the Soluble Epoxide Hydrolase as an Analgesic Strategy: A Review of Preclinical Evidence. J Pain Res 2021, 14, 61–72. [PubMed: 33488116]

67. Finn DP; Haroutounian S; Hohmann AG; Krane E; Soliman N; Rice ASC, Cannabinoids, the endocannabinoid system, and pain: a review of preclinical studies. Pain 2021, 162 (Suppl 1), S5–s25. [PubMed: 33729211]

68. Guindon J; Hohmann AG, The endocannabinoid system and pain. CNS Neurol Disord Drug Targets 2009, 8 (6), 403–21. [PubMed: 19839937]

69. Clapper JR; Moreno-Sanz G; Russo R; Guijarro A; Vacondio F; Duranti A; Tontini A; Sanchini S; Sciolino NR; Spradley JM; Hohmann AG; Calignano A; Mor M; Tarzia G; Piomelli D, Anandamide suppresses pain initiation through a peripheral endocannabinoid mechanism. Nat Neurosci 2010, 13 (10), 1265–70. [PubMed: 20852626]

70. Walker JM; Huang SM; Strangman NM; Tsou K; Sañudo-Peña MC, Pain modulation by release of the endogenous cannabinoid anandamide. Proc Natl Acad Sci U S A 1999, 96 (21), 12198–203. [PubMed: 10518599]

71. Totrov M, Atomic property fields: generalized 3D pharmacophoric potential for automated ligand superposition, pharmacophore elucidation and 3D QSAR. Chem Biol Drug Des 2008, 71 (1), 15–27. [PubMed: 18069986]
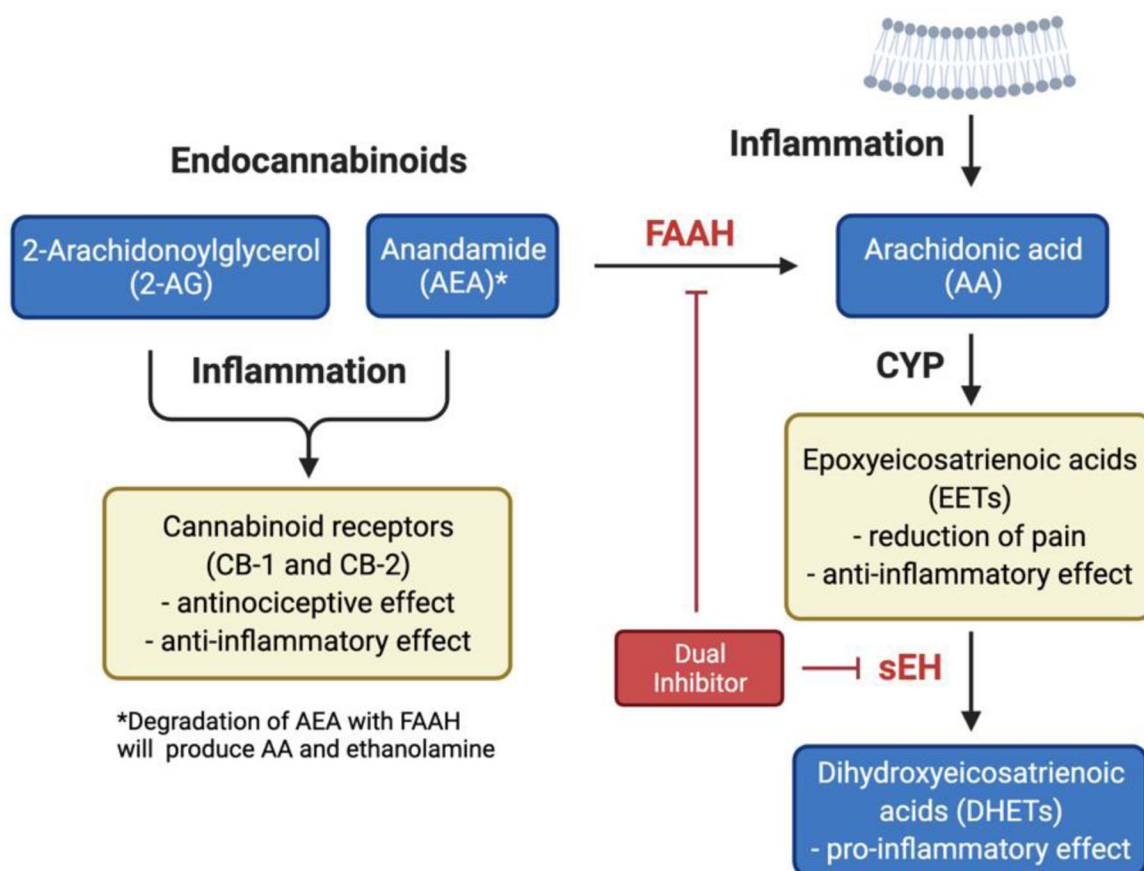
**Figure 1.**
Metabolic pathways of enzymes fatty acid amide hydrolase and soluble epoxide hydrolase and interactions with arachidonic acid.
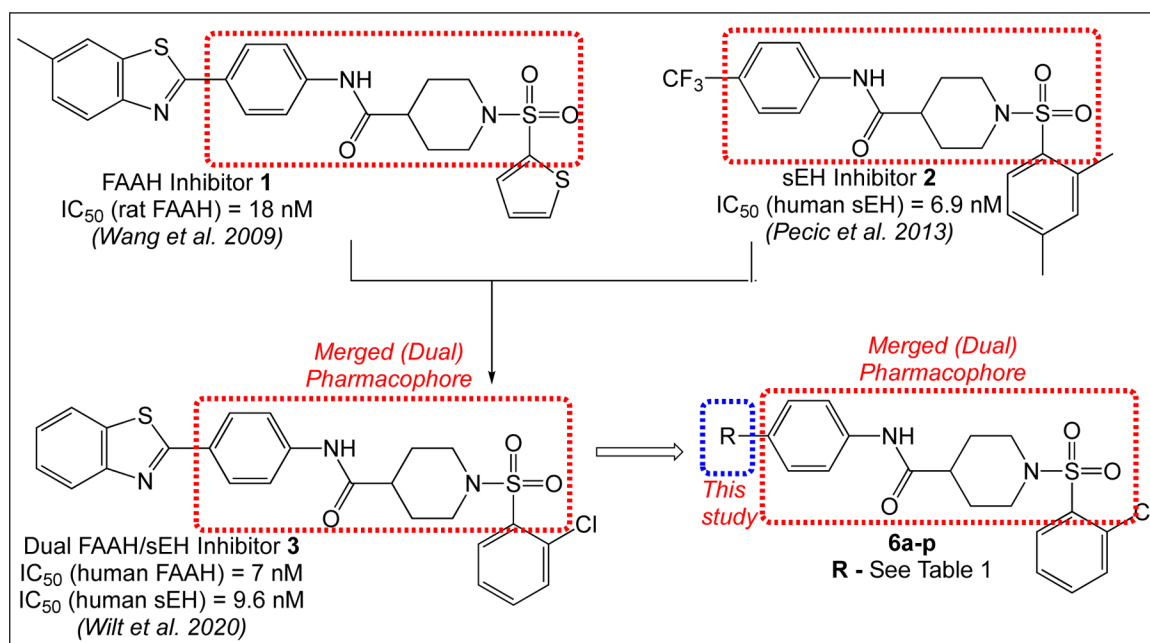
**Figure 2.**
Design strategy used to optimize new dual FAAH/sEH inhibitors. Key pharmacophoric features required to interact with both targets are merged in one united pharmacophore (shown in red box). The site of interest where SAR is performed in this study is shown in blue box.
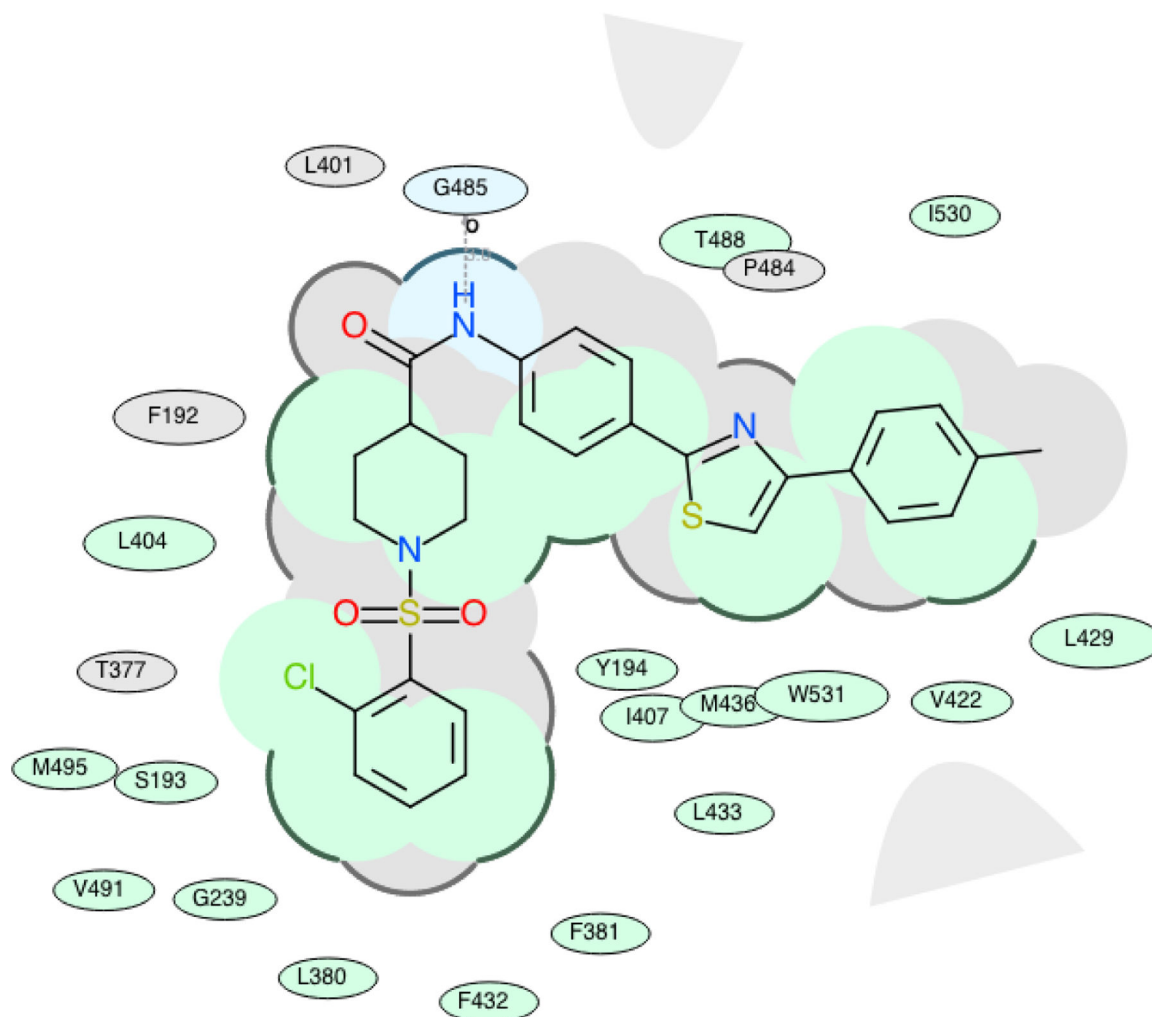
**Figure 3A.**
Binding of **6o** in human FAAH active site (2D representation): green shading represents hydrophobic regions; gray parabolas represent accessible surfaces for large areas; gray dotted lines represent hydrogen bonds; broken thick line around **6o** shape indicates accessible surfaces; size of residue ellipse represents the strength of the contact.
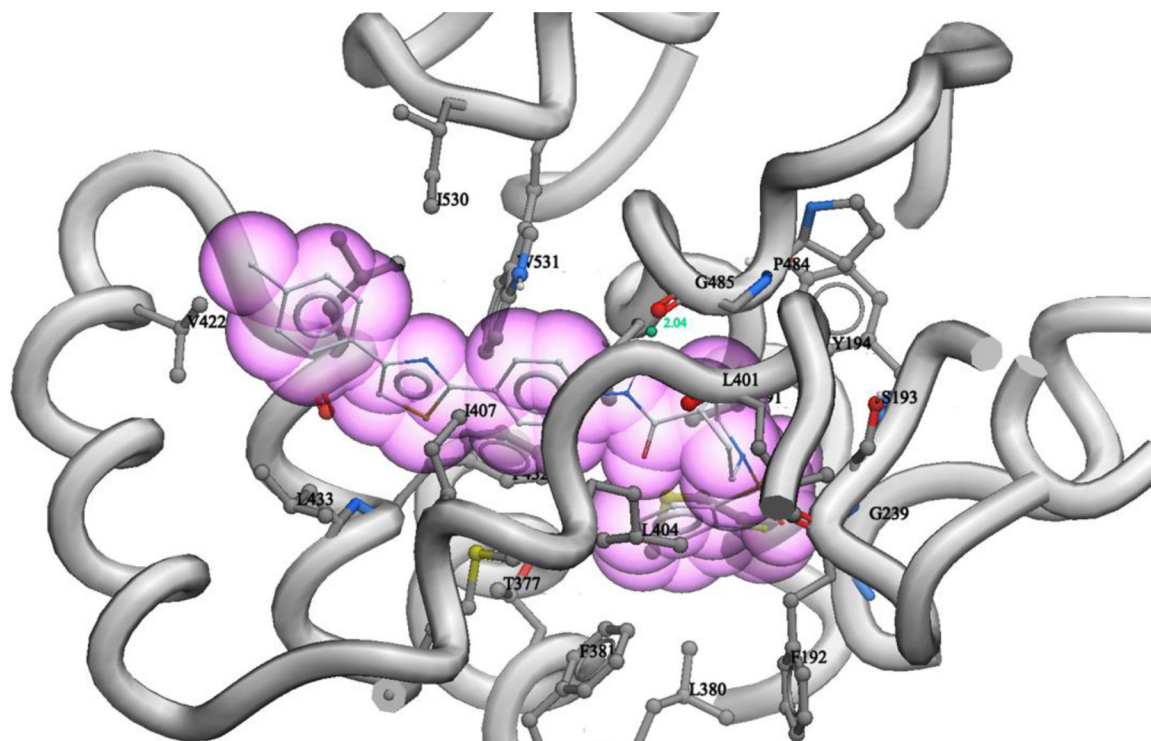
**Figure 3B.**

Binding of **6o** in human FAAH active site (3D representation): Important amino acid residues in the proximity of **6o** are shown and labeled. Hydrogen bond with G485 is shown in green with the distance in Å.
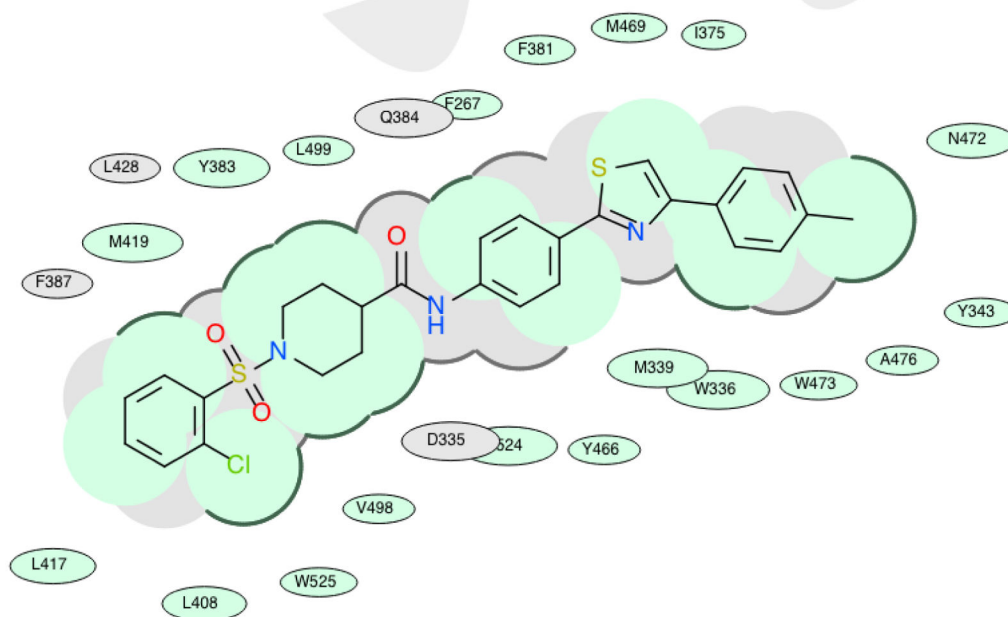
**Figure 4A.**
Binding of **6o** in human sEH active site (2D representation): green shading represents hydrophobic regions; gray parabolas represent accessible surfaces for large areas; gray dotted lines represent hydrogen bonds; broken thick line around **6o** shape indicates accessible surfaces; size of residue ellipse represents the strength of the contact.
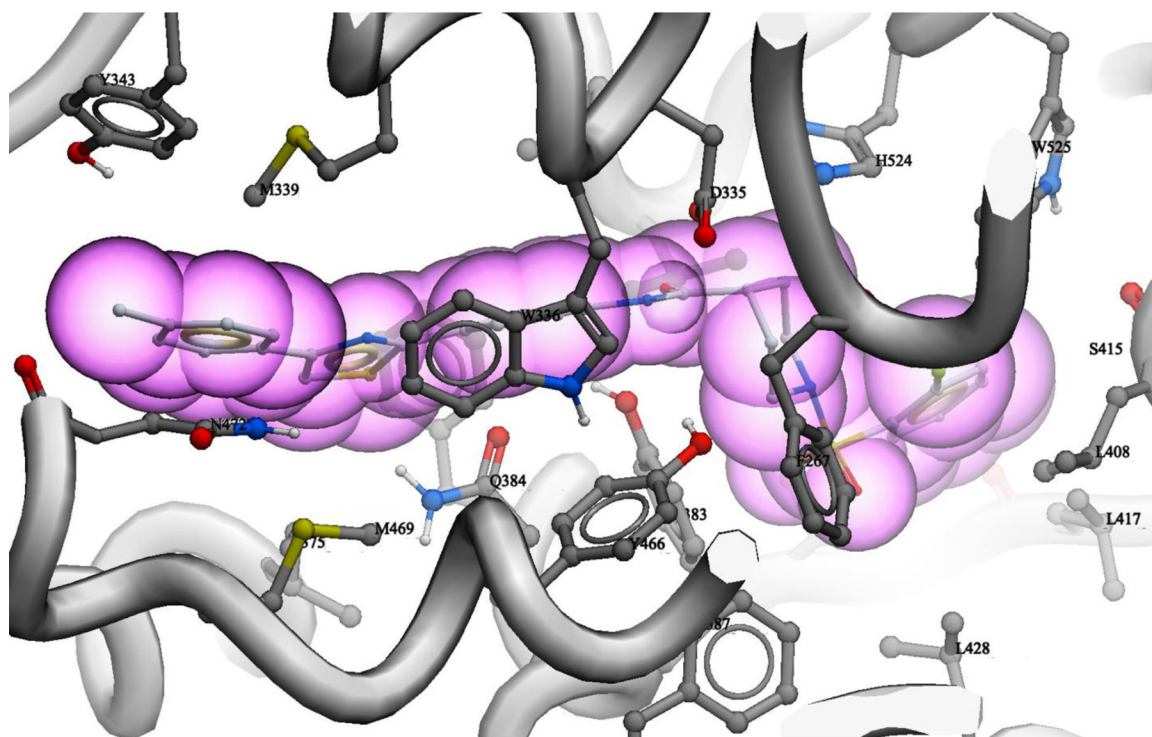
**Figure 4B.**
Binding of **6o** in human sEH active site (3D representation): Important amino acid residues in the proximity of **6o** are shown and labeled.
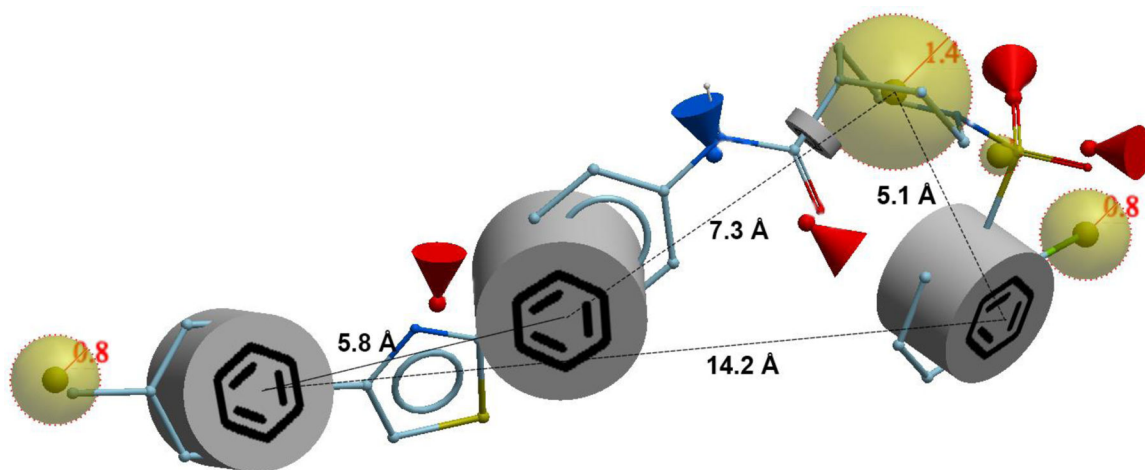
**Figure 5.**
Proposed pharmacophore for dual inhibitors based on the binding of **60** in both FAAH and sEH enzymes. Potential hydrogen bond donors are represented with blue cone, hydrogen bond acceptors with red cones, the lipophilic part of the molecule are shown as yellow spheres and aromatic parts are shown as grey barrels. The distances between major pharmacophoric parts are represented with dotted lines.

**A**

## Phase 1 (0-10 min)



**B**

## Phase 2 (20-60 min)
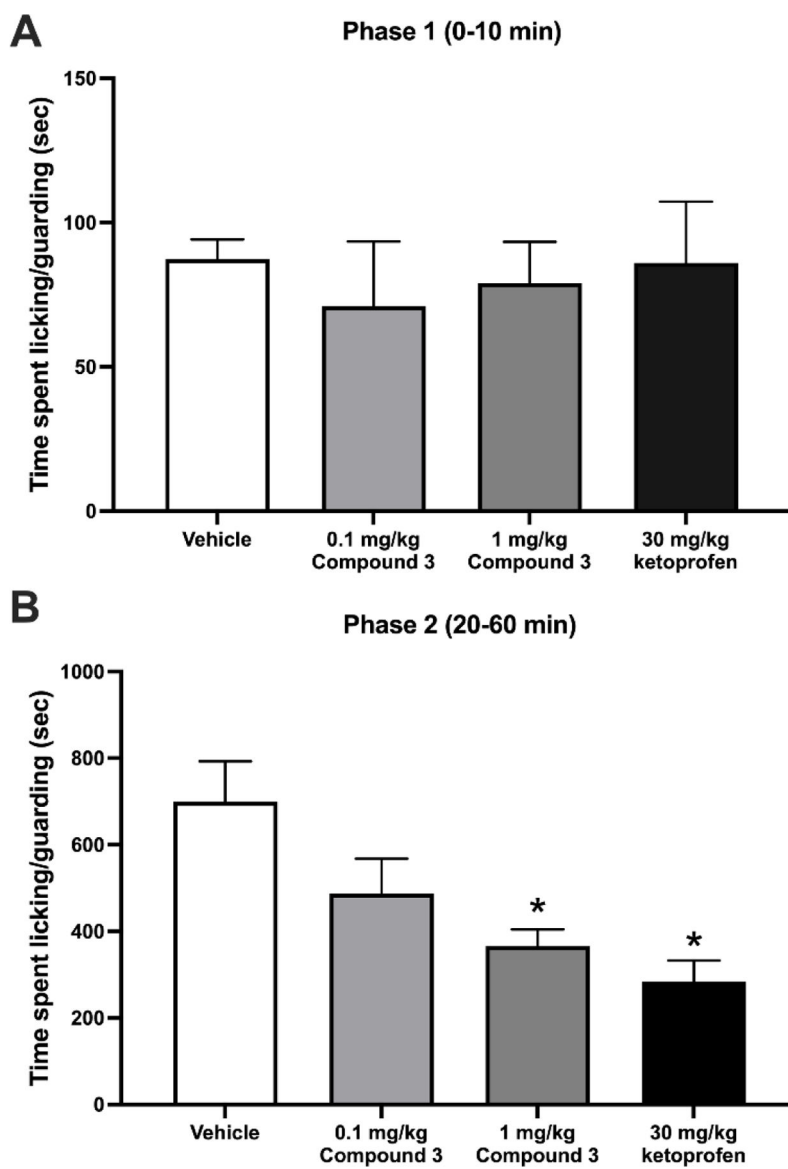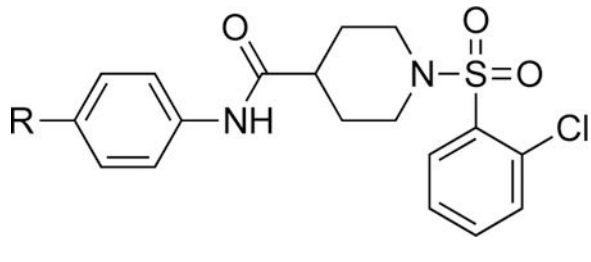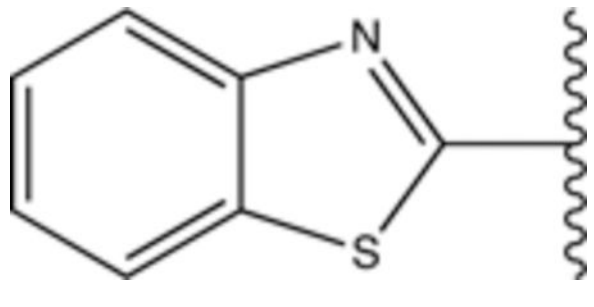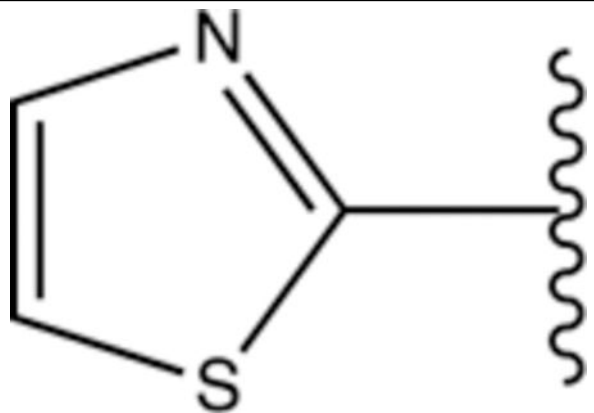


**Figure 6. Antinociceptive effects of 3 against formalin-induced inflammatory pain.**
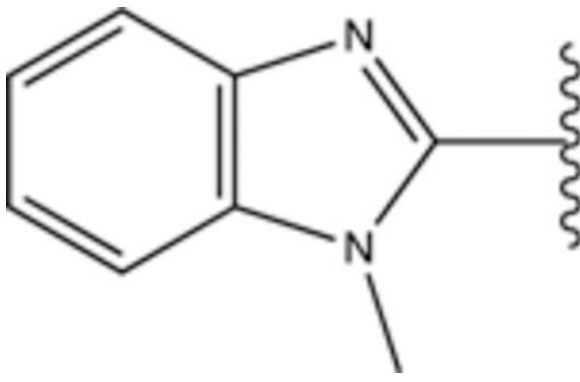A) Pain-related behaviors (licking and guarding of the injected hindpaw) in the first phase of the Formalin Test. B) Pain-related behaviors in the second phase of the Formalin Test. n = 6/group. * indicates $p < 0.05$ from vehicle-treated rats.
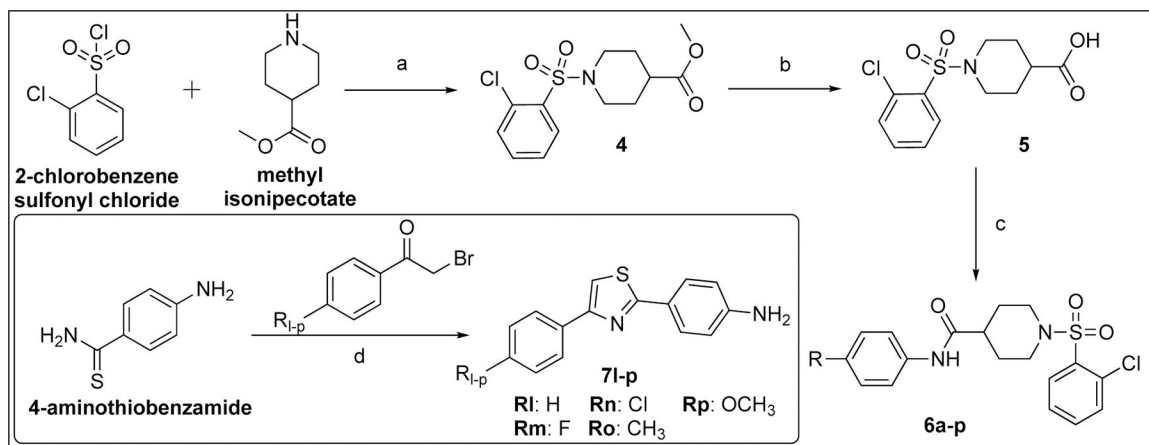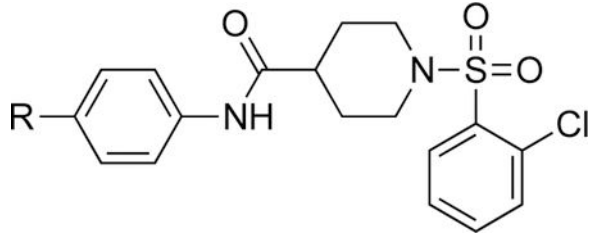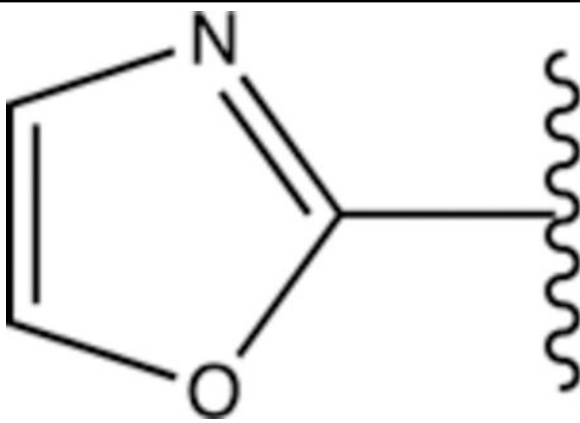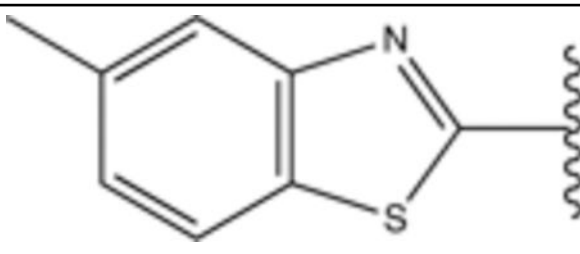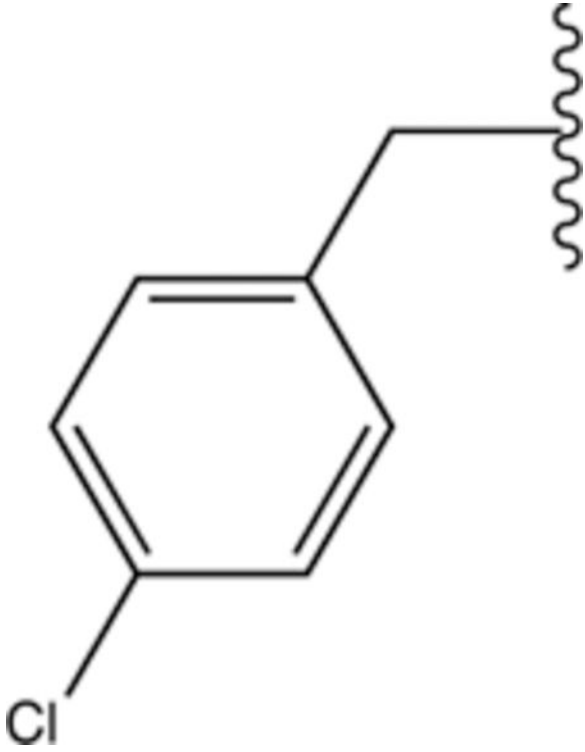
**Scheme 1.**
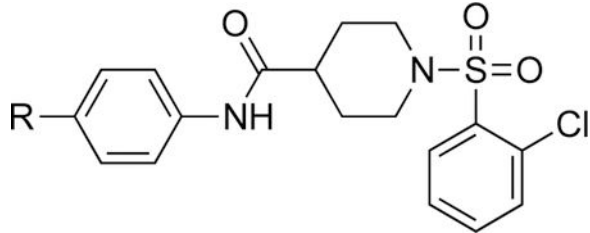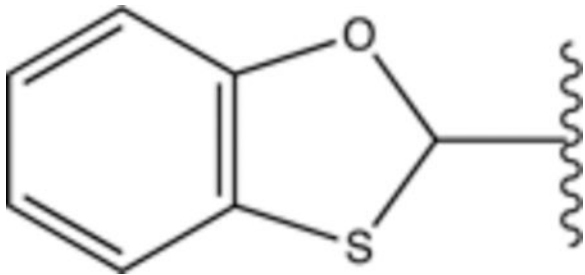
*Reagents and conditions:* (a) DIPEA, DCM, 20 min, 80 °C, microwave irradiation, 74%; (b) LiOH/H2O, 16 h, rt, TFA, DCM, rt, 24 h, 91%; (c) **7l-p** (see the inner box) or R-aniline (see Table 1 for R), EDC, DMAP, DCM, 20 min, 80 °C, microwave irradiation, 24–91%; (d) iPrOH, 2.5 h, 60 °C, 57–95%.
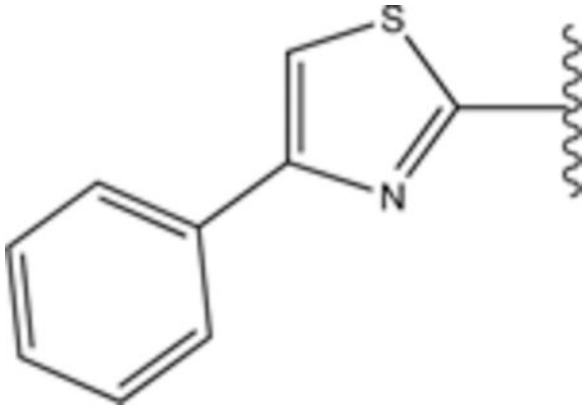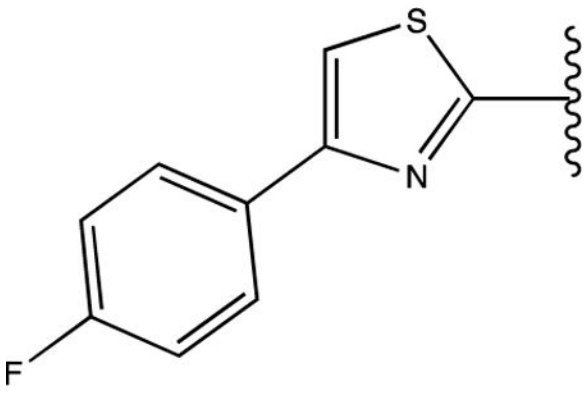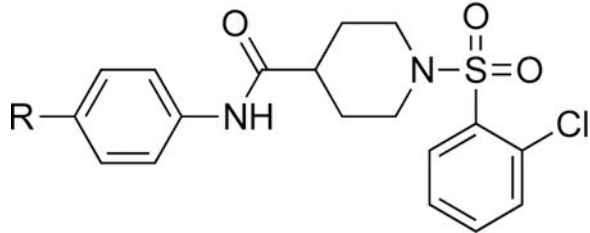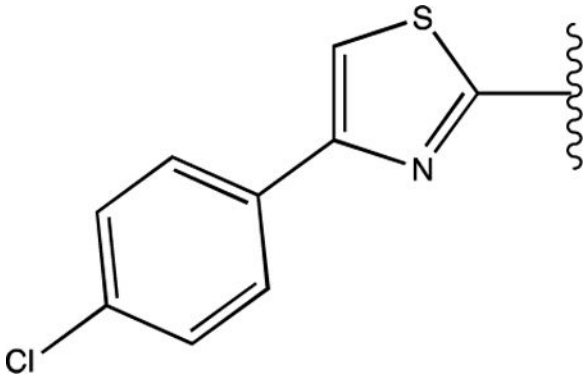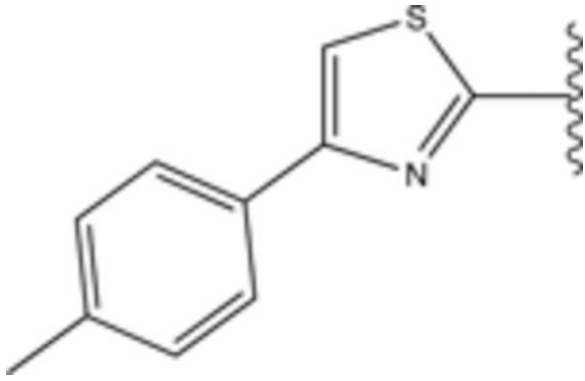
**TABLE 1.**
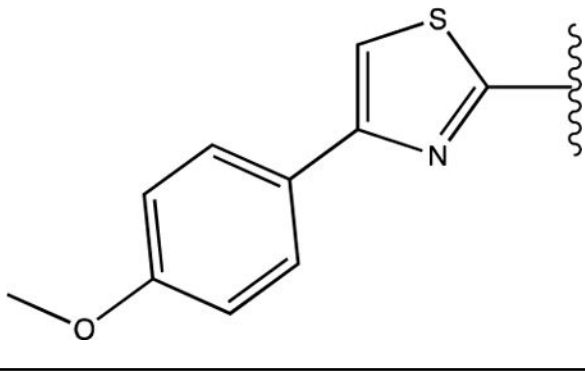
Fatty acid amide hydrolase (FAAH) and soluble epoxide hydrolase (sEH) inhibitory activities and docking scores of analogs



| Compound | R | FAAH IC$_{50}$ (nM)$^{a,b}$ | sEH IC$_{50}$ (nM) $^{a,b}$ | Docking Score FAAH | Docking Score sEH |
|---|---|---|---|---|---|
| URB 597 | - | 32 | - | −31.45 | −22.16 |
| AUDA | - | - | 1.9 | −22.18 | −25.83 |
| 3 |  | 7 | 9.6 | −28.93 | −33.03 |
| 6a | −H | 510 | >10000 | −19.43 | −24.71 |
| 6b | −F | 220 | >10000 | −20.90 | −25.99 |
| 6c | −Cl | 160 | >10000 | −20.50 | −27.11 |
| 6d | −Br | 130 | >10000 | −20.89 | −27.85 |
| 6e | −CH$_3$ | 110 | >10000 | −22.50 | −28.05 |
| 6f |  | 102 | 9.2 | −28.02 | −22.56 |

| | | | | | |
|---|---|---|---|---|---|
| | | | |  | |

| Compound | R | FAAH IC$_{50}$ (nM)$^{a,b}$ | sEH IC$_{50}$ (nM) $^{a,b}$ | Docking Score FAAH | Docking Score sEH |
|---|---|---|---|---|---|
| 6g |  | 140 | 180 | −21.14 | −26.43 |
| 6h |  | 1.8 | 8.7 | −31.42 | −28.90 |
| 6i |  | 330 | 1400 | −28.87 | −23.19 |

| Compound | R | FAAH IC$_{50}$ (nM)$^{a,b}$ | sEH IC$_{50}$ (nM) $^{a,b}$ | Docking Score FAAH | Docking Score sEH |
|---|---|---|---|---|---|
| 6j | | 142 | 22.7 | −17.62 | −25.98 |
| 6k | | >10000 | 170 | −20.65 | −24.72 |

| Compound | R | FAAH IC$_{50}$ (nM)$^{a,b}$ | sEH IC$_{50}$ (nM) $^{a,b}$ | Docking Score FAAH | Docking Score sEH |
|---|---|---|---|---|---|
| 6l |  | 30.8 | 3.1 | −30.69 | −33.58 |
| 6m |  | 18.2 | 2.4 | −26.57 | −33.19 |

| Compound | R | FAAH IC$_{50}$ (nM)$^{a,b}$ | sEH IC$_{50}$ (nM) $^{a,b}$ | Docking Score FAAH | Docking Score sEH |
|---|---|---|---|---|---|
| |  | | | | |
| 6n |  | 25.1 | 9.6 | −30.65 | −33.39 |
| 6o |  | 9.8 | 2.5 | −33.54 | −31.14 |
| 6p |  | 11.1 | 2.3 | −30.50 | −30.60 |

[a]Reported $IC_{50}$ values are the average of three replicates. The fluorescent assay as performed here has a standard error between 10 and 20% suggesting that differences of two fold or greater are significant.[44]

[b]$t$-AUCB and PF-3845 that have an $IC_{50}$ between 1 and 2 nM were used as positive controls for sEH and FAAH assays, respectively.[45, 46]

**TABLE 2.**

Predicted ADMET properties for selected dual sEH/FAAH inhibitors

| | Mol Weight | cLogP | N of HBA | N of HBD | PSA | N of Rot Bonds | Caco-2 | Half Life (h) | hERG | LD50 | Tox Score | Drug Likeness |
|---|---|---|---|---|---|---|---|---|---|---|---|---|
| **6h** | 526.066 | 5.39 | 8 | 1 | 64.5 | 6 | −5.32 | 1.95 | 0.25 | 399.22 | 0 | 0.33 |
| **6l** | 538.0770 | 5.68 | 8 | 1 | 64.5 | 7 | −5.19 | 1.91 | 0.18 | 435.06 | 0 | 0.81 |
| **6m** | 556.0674 | 5.86 | 8 | 1 | 64.5 | 7 | −5.26 | 2.26 | 0.29 | 439.39 | 0 | 0.96 |
| **6n** | 572.5190 | 6.39 | 8 | 1 | 64.5 | 7 | −5.25 | 2.26 | 0.21 | 444.02 | 0 | 0.98 |
| **6o** | 552.1040 | 6.24 | 8 | 1 | 64.5 | 7 | −5.21 | 2.26 | 0.25 | 449.33 | 0 | 0.70 |
| **6p** | 568.1030 | 5.75 | 9 | 1 | 72.04 | 8 | −5.13 | 3.04 | 0.39 | 440.99 | 0 | 0.94 |